Bioinspired Cable-Driven Actuation System for Wearable Robotic Devices: Design, Control, and Characterization

Ming Xu, *Graduate Student Member, IEEE*, Zhihao Zhou, *Member, IEEE*, Zezheng Wang, Lecheng Ruan, Jingeng Mai, and Qining Wang, *Senior Member, IEEE*

***Abstract*—Wearable robotic devices interact with humans by applying the assistive force in parallel with muscle–tendon systems. Designing actuations in mimicking the natural activation patterns of human muscles is a promising way to optimize the performance of wearable robots. In this article, we propose a bioinspired cable-driven actuation system capable of providing anisometric contractions (including concentric and eccentric contraction) assistance or nearly acting as a transparent device in an efficient manner. A novel clutch–spring mechanism is employed to accomplish switches between assistive modes and the transparent mode. Corresponding control strategies coordinating with the mechanical design were presented and described in detail. Multiple evaluations were conducted on a test bench to characterize the system's performance. The closed-loop bandwidth of the system running concentric assistance control was 18.2 Hz. The *R*-squared values of linear fitting under eccentric assistance control were above 0.99. The engagement time of the proposed clutch was about 90 ms. Applying the actuation to an ankle exoskeleton, multiple walking experiments with electromyography measurements were performed on five subjects to show its application potential in existing wearable robots. Experimental results revealed that the proposed design could reduce soleus muscle activity by 27.32% compared with normal walking. This study highlights the importance of functional bionic design in human-assistance-related devices and introduces a general actuation system that could be directly applied to existing cable-driven wearable robots.**

***Index Terms*—Actuation system, bioinspired, cable driven, wearable robotic device.**

Manuscript received 8 July 2023; accepted 2 October 2023. Date of publication 16 October 2023; date of current version 15 December 2023. This paper was recommended for publication by Associate Editor S. Crea and Editor A. Menciassi upon evaluation of the reviewers' comments. This work was supported by the National Natural Science Foundation of China under Grant 52005011, Grant 52375001, and Grant 91948302. *(Ming Xu and Zhihao Zhou contributed equally to this work.) (Corresponding author: Qining Wang.)*

This work involved human subjects or animals in its research. Approval of all ethical and experimental procedures and protocols was granted by the Local Ethics Committee of Peking University, China, under Application 2018-06-02.

Ming Xu, Zezheng Wang, and Jingeng Mai are with the Department of Advanced Manufacturing and Robotics, College of Engineering, and the Institute for Artificial Intelligence, Peking University, Beijing 100871, China, and also with the Beijing Engineering Research Center of Intelligent Rehabilitation Engineering, Beijing 100871, China (e-mail: xuming@stu.pku.edu.cn; zezhengwang@stu.pku.edu.cn; jingengmai@pku.edu.cn).

Zhihao Zhou is with the Institute for Artificial Intelligence, Peking University, Beijing 100871, China, and also with the Beijing Engineering Research Center of Intelligent Rehabilitation Engineering, Beijing 100871, China (e-mail: zhouzhihao@pku.edu.cn).

Lecheng Ruan is with the National Key Laboratory of General Artificial Intelligence, Beijing Institute for General Artificial Intelligence (BIGAI), Beijing 100080, China (e-mail: ruanlecheng@bigai.ai).

Qining Wang is with the Department of Advanced Manufacturing and Robotics, College of Engineering, and the Institute for Artificial Intelligence, Peking University, Beijing 100871, China, also with the Peking University Third Hospital, Beijing 100191, China, also with the University of Health and Rehabilitation Sciences, Qingdao 266071, China, and also with the Beijing Institute for General Artificial Intelligence, Beijing 100080, China (e-mail: qiningwang@pku.edu.cn).

This article has supplementary material provided by the authors and color versions of one or more figures available at https://doi.org/10.1109/TRO.2023.3324200.

Digital Object Identifier 10.1109/TRO.2023.3324200

I. Introduction

WEARABLE robotic devices, such as robotic exoskeletons or orthoses, have attracted increasing interest and have been greatly advanced over the past two decades [1], [2], because of their significant functionalities in human performance augmentation, impaired individual assistance, and motor rehabilitation [3]. These robotic devices are designed to interact with the human body by applying the assistive force in parallel with muscle–tendon systems and replace the functionalities of musculoskeletal systems partially or entirely [4]. As the power source of wearable robotic devices, the actuation system serves as the human muscle. According to the principle of functional bionic design, it is a promising way to optimize the performance of wearable robots by imitating natural biomechanical characteristics of human muscles efficiently.

Generally, the natural activation patterns of human muscles include isometric contraction and anisometric contractions [5]. Isometric contraction refers to the muscle activation at constant length without power output [6]. The main functionality of isometric contraction is to support and maintain body posture. Anisometric contractions with power output can be divided into concentric contraction and eccentric contraction, according to the direction of the muscle length variation [7]. In concentric contraction, the contractile force in the muscle decreases as the muscle length shortens under load [8]. During this process, the direction of the muscle velocity is in accord with that of the muscle contractile force, and the muscle does positive work to actuate the human body. For instance, in the push-off period of bipedal walking, the soleus contracts concentrically to generate propulsion [6]. In eccentric contraction, the muscle length increases under load; meanwhile, the direction of the muscle contractile force is against that of the muscle velocity [9]. The muscle does negative work to reduce the moving velocity

of the human body during eccentric contraction. For example, in the midstance period of bipedal walking, the ankle joint dorsiflexes passively resulted from the forward movement of the body weight. In this process, the soleus contracts eccentrically to generate a resistive moment preventing the ankle joint from rotating too fast and ensuring the body weight moves forward smoothly [10]. In the stand-to-sit transition, the quadriceps femoris contracts eccentrically to provide a resistive moment preventing the human body from falling too fast under gravity [11]. Overall, to supply motion assistance for the humans, the actuation system of wearable robotic devices is expected to act like anisometric contractions of human muscles.

Besides, according to the "assist-as-needed" principle, the wearable robot is also expected to follow the natural motion of the human body as transparently as possible in some cases [12]. For instance, in the swing phase of the gait cycle during level-ground walking, the ankle joint does not need to support the human body and the biomechanical ankle moment decreases substantially [8]. Meanwhile, the ankle joint rotates freely to prepare for the next ground contact. Wearable robots are expected to exert minimized interaction force on the human in this period [13], [14], [15]. However, to improve the output torque of wearable robots, the reducer with a high reduction ratio is generally employed in the actuation design, which will deteriorate the back-drivability of the robotic system [16]. How to achieve system transparency effectively is a big challenge in implementation [17], [18].

To date, for mimicking the anisometric contractions of human muscles and achieving system transparency, plenty of efforts have been made by researchers all over the world. In terms of mechanical transmission, the cable has been applied generally in the actuation system of wearable robotic devices, e.g., exoskeletons for the hip joint [19], knee joint [20], ankle joint [15], upper limb [21], [22], [23], and the hand [24]. Because it achieves power transmission by changing the distance between two anchors, which is similar to muscle contraction. And the cable transmission has outstanding advantages in lightweight, power efficiency, simplicity, and flexibility of design compared with other mechanical transmissions [25], [26].

In terms of functionality, researchers have tried to imitate the anisometric contractions of human muscles and achieve system transparency in several ways.

1) On the one hand, many powered devices based on cable transmission were proposed to meet this goal. They utilized brushless dc motor driving pulleys directly to exert active assistance on the human, no matter in the concentric or eccentric assistance period [14], [15], [27], [28], [29], [30]. These designs are simple in mechanical structure and driving strategy, yet will consume unnecessary electrical power for actuating the motor actively during eccentric assistance. In [27], commanding the motor to stay at a fixed position was also with nonignorable electrical energy consumption, although the eccentric assistance force was passively generated by the natural ankle dorsiflexion. In these designs, Slade [15], Quinlivan [14], and Chen [30] achieved complete system transparency through cable slack management, i.e., pushing the cable out to slack during nonassistive phase [31]. However, due to the friction in transmission, slackening may cause the cable to derail from the pulley, resulting in system failure [32]. Park [28] and Schmidt [29] tried to minimize the human–robot interaction by commanding a "zero-torque" control, but the control performance was limited to the system bandwidth. In other words, the human–robot interaction force would enlarge with the increase in human motion frequency [33], [34].
2) On the other hand, Collins et al. [13] designed a passive spring–clutch mechanism to imitate the activation patterns of calf muscles. In this design, the clutch engaged a parallel spring with the human ankle in the stance phase of the gait cycle to supply eccentric assistance (in the midstance period) and concentric assistance (in the push-off period) while disengaged in the swing phase to allow free motion. This passive device can simulate two anisometric activation patterns of calf muscles and achieve transparency through clutch disengagement. However, this passive design is only suitable for the fixed application scenario, i.e., ankle assistance in level-ground walking. Moreover, the assistance force profile cannot be adjusted in real time. The switching orders of different action modes fully depend on the mechanical structure, and the mechanism needs to be customized according to the body figure of the wearer. By contrast, Shepertycky et al. [20] proposed a passive device to provide only eccentric assistance for the hamstrings during the terminal swing phase of the gait cycle. In this passive device, the assistance force profile could be adjusted through generator internal resistance regulation, but only one contraction assistance pattern was involved.
3) Besides, other efforts have been made in wearable robots with rigid structures [35], [36], [37]. They integrated series electromechanical/magnetic clutches into the robotic design. These devices can provide active or passive assistance when clutches are engaged and achieve transparent mode by decoupling the driving motor with the robotic joint. However, employing an electromechanical/magnetic clutch introduces another power source for clutch control and may increase the size, inertia, and control complexity of the robotic system.

Overall, most existing designs could provide anisometric contraction assistance by commanding the motor to rotate actively, yet consuming extra electrical power to assist eccentric contraction is unnecessary. Given the force–velocity characteristic of eccentric contractions, it is more efficient to generate corresponding assistive force from electromagnetic induction. Moreover, despite these efforts to achieve system transparency, there remain limitations to avoiding cable derailment and performance deterioration.

To address these issues, in this article, we propose a bioinspired cable-driven actuation system that integrates both anisometric contractions assistance and transparent mode. In this design, the generator status is utilized to supply eccentric assistance, and a clutch–spring mechanism controlled by the driving motor is employed to quickly switch between assistive modes and the transparent mode. Corresponding control strategies coordinating with the mechanical design are presented and

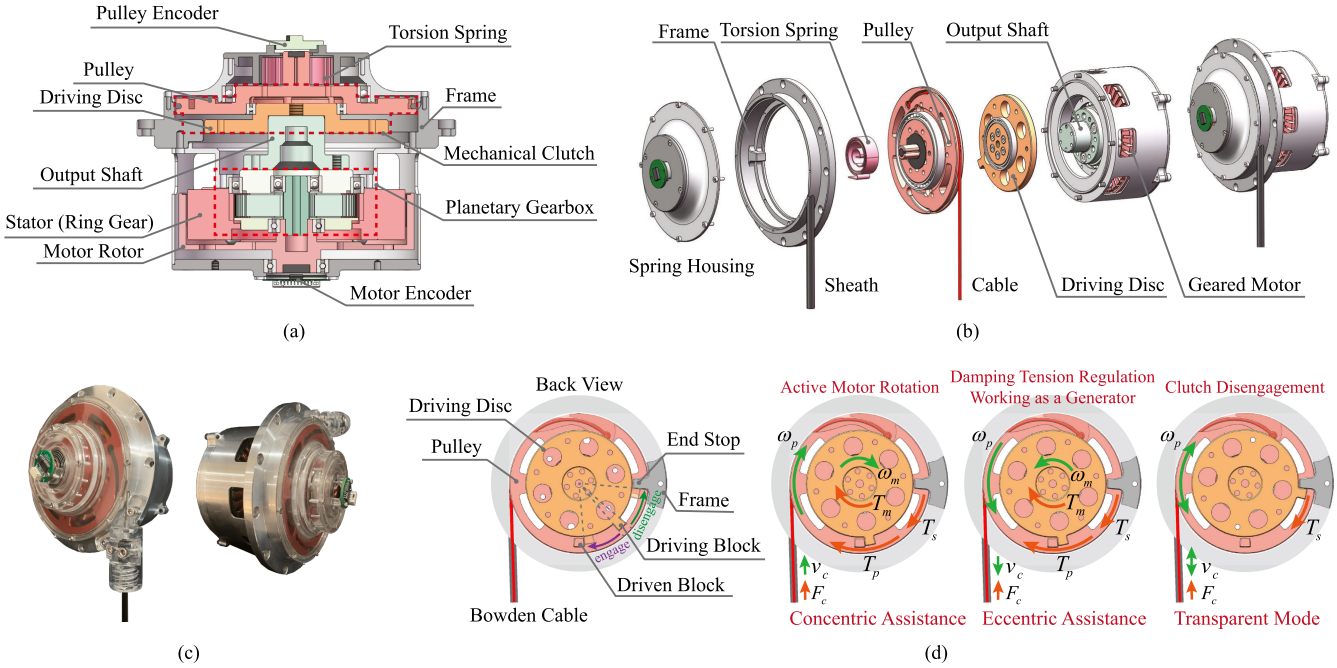

Fig. 1. Actuation system design. The bioinspired cable-driven actuation system is capable of supplying concentric assistance (by active motor rotation) and eccentric assistance (by damping tension regulation) according to the activation status of human muscles, or nearly acting as a transparent device (by clutch disengagement) when assistance is not needed. The mode switches between assistive modes and the transparent mode fully depends on the mechanical clutch controlled by the driving motor. In this figure, ω_m and T_m are the angular velocity and the output torque of the motor, respectively; ω_p and T_p are the angular velocity and the output torque of the pulley, respectively. T_s refers to the torque provided by the torsion spring. v_c and F_c represent the velocity and the force of the cable, respectively. (a) Cross-sectional view of the mechanical design. (b) Explosive view of the mechanical design. (c) Implementation photos. (d) Working principles of the actuation system.

implemented. Both test bench evaluations and walking experiments with electromyography (EMG) measurements performed on an ankle exoskeleton were conducted to characterize its performance.

The rest of this article is organized as follows. The mechanical design and synergy mechanism of the actuation system are shown in Section II. The control strategies are presented in Section III. Section IV illustrates the performance characterization of the proposed actuation. Section V describes the wearable robot application tests while Section VI presents the EMG evaluation experiments. Section VII presents the discussion. Finally, Section VIII concludes this article.

II. Actuation System

According to the natural biomechanical characteristics of human muscles, a bioinspired cable-driven actuation system that integrates three action modes is proposed. This device can cooperate with human muscles to provide concentric assistance (by active motor rotation), eccentric assistance (by damping tension regulation), or nearly act as a transparent system (by clutch disengagement), in the proper period. The mechanical design of the actuation system and the synergy mechanism between the actuation and the human muscle are described in this section.

A. System Design

As shown in Fig. 1, a compact cable-driven actuation system that integrates three action modes and employs a clutch–spring mechanism to quickly achieve mode switches is proposed to mimic the biomechanical characteristics of human muscles. The Bowden cable composed of inner steel cable (diameter: 1.5 mm, capacity: 220 lb) and outer sheath (external diameter: 5 mm, internal diameter: 2 mm) is selected as the transmission medium. Fig. 1(a) shows the cross-sectional mechanical structure and Fig. 1(b) illustrates the explosive view of the proposed actuation system. In this design, the mechanical power is generated by a brushless dc motor with a 6:1 planetary gearbox (weight 0.54 kg, rated torque 8 N · m, peak torque 16 N · m, rated speed 300 r/min, SS-BLDC-6-300, SpeedSmart Company, Ltd., China), which is electrically powered by a Li-ion battery (48 V, 2600 mAh). The geared motor drives a clutch–spring mechanism through the output shaft. The clutch–spring mechanism refers to the unidirectional mechanical clutch parallel with a torsion spring. The unidirectional mechanical clutch consists of three major parts: 1) the driving disc with a driving block, 2) the 43.5-mm radius single-wrap pulley with a driven block, and 3) the frame with an end stop. The stator of the dc motor mounted on the frame is housed by the motor rotor, and the ring gear of the planetary gearbox is integrated into the stator of the dc motor for mechanical simplicity. The output shaft connects the planet carrier of the planetary gearbox with the driving disc of the mechanical clutch while the pulley is mounted between the driving disc and the frame through bearings. A pretensioned torsion spring connects the pulley to the frame. The torsion spring wraps around the central shaft of the pulley while one end of the torsion spring is attached to the central shaft of the pulley and the other is fixed on the frame. When

the cable is unspooled, the torsion spring will be compressed, and the consequential spring force is capable of ensuring that the cable is in tension, for avoiding mechanical failure of the cable stuck and making the transmission more compliant [38]. Besides, the rotation information of the motor and the pulley are captured by two magnetic encoders mounted along the motor shaft and pulley shaft, respectively. Apart from encoders, the control hardware of the actuation also includes a motor driver and a custom electronics board with functions of data acquisition and control. Overall, the entire length of the actuation system is 86 mm (plus the thickness of encoders), the maximum diameter is 118 mm, and the weight is about 1.10 kg.

The switching process between assistive modes (concentric assistance and eccentric assistance) and the transparent mode mainly depends on the unidirectional mechanical clutch. As shown in Fig. 1(d), the driving block of the driving disc is arranged between the driven block of the pulley and the stop block of the frame. On the one hand, if the driving disc clockwise rotates driven by the motor until the driving block of the driving disc contacts with the driven block of the pulley, the clutch will engage the pulley with the motor. After the clutch engagement, if the motor continues to clockwise rotate actively, the cable will be spooled into the slot of the pulley. In this case, the mechanical power generated by the motor can be transmitted to the object, and the actuation is capable of providing concentric assistance (active motor rotation). Contrariwise, after the clutch engagement, if the motor anticlockwise rotates passively pulled by the object, the cable will be unspooled from the slot of the pulley. In this case, the motor will work as a generator to generate braking torque resulting from the induced current, and the actuation is capable of providing eccentric assistance (damping tension regulation). On the other hand, if the driving disc anticlockwise rotates actively driven by the motor until the driving block of the driving disc is decoupled with the driven block of the pulley, the clutch will be disengaged. After clutch disengagement, the cable is decoupled with the motor and, thus, can be spooled or unspooled passively only under the effects of the pretensioned torsion spring (clutch disengagement). When the driving disc anticlockwise rotates actively driven by the motor until the driving block of the driving disc contacts with the stop block of the frame, the pulley can rotate with the maximal range of approximately 330° without motor interference. Meanwhile, the maximum free motion range of the cable is achieved (about 250 mm).

B. Synergy Mechanism

The actuation system is designed to cooperate in parallel with the muscle–tendon system of the human to reduce muscle activation. In this device, the assistive modes include both concentric and eccentric assistance. The mode switches between assistive modes and the transparent mode are achieved by the clutch status control. Taking soleus as an example (see Fig. 2), the synergy mechanisms between the proposed actuation and the human muscle are illustrated as follows.

1) Concentric Assistance: In the concentric contraction period of the soleus (mainly in the push-off period of the human gait cycle), the mechanical clutch engages the pulley with the motor, and the mechanical power actively generated by the actuation will be transferred to the user's leg to achieve concentric assistance concerning plantarflexion aid.

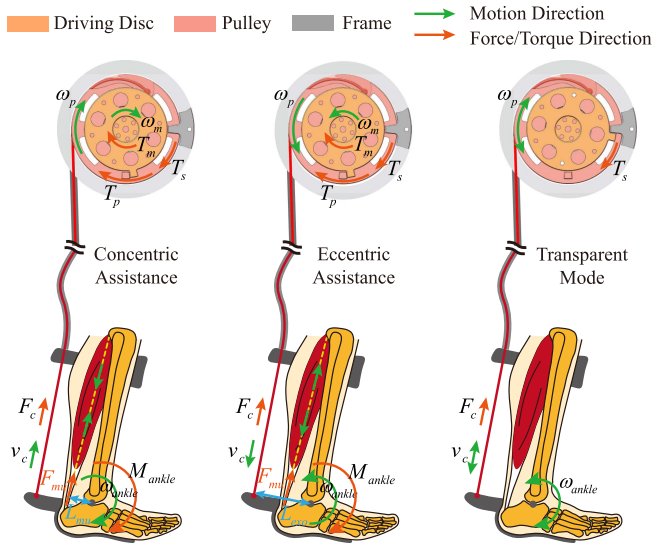

Fig. 2. Synergy mechanisms between the proposed actuation and the human muscle (taking soleus as an example). In assistive modes, the proposed actuation cooperates with the human muscle and reduces muscle activation by applying proper assistive force in parallel with the corresponding muscle–tendon system. In the transparent mode, the interaction torque between the device and the human fully depends on the pretension level of the torsion spring. In this figure, F_{mu} is the muscle force generated by the soleus, and L_{mu} symbolizes the moment arm of the muscle force relative to the CoR of the ankle joint. L_{exo} refers to the moment arm of the cable force generated by the actuation system. ω_{ankle} and M_{ankle} represent the angular velocity and the moment of the human ankle, respectively.

During this process, the pulley rotates with the motor, thus

$$\omega_p = \omega_m \tag{1}$$

where ω_p refers to the angular velocity of the pulley, and ω_m refers to the angular velocity of the motor.

The torque generated by the actuation and exerted on the pulley can be expressed as

$$T_p = T_m + T_s \tag{2}$$

where T_p and T_m are the output torque of the pulley and the motor, respectively. T_s is the torque provided by the torsion spring.

In this design, the friction of bearings is insignificant compared with that of Bowden cable; thus, can be neglected in the analysis.

According to the principle of power conservation, we can obtain

$$T_p \omega_p = F_c v_c \eta_B \tag{3}$$

where F_c and v_c represent the tensile force and the velocity of the cable, respectively. η_B represents the efficiency of the Bowden cable transmission.

According to the Capstan formula [39], [40], [41], the efficiency of the Bowden cable transmission can be

modeled as

$$\eta_B = e^{\mu\theta} \tag{4}$$

where μ is the coefficient of kinetic friction between the sheath and the cable, and θ is the curve angle of the entire Bowden cable.

By combining (1), (2), (3), and (4), we can obtain the cable force

$$F_c = \frac{(T_m + T_s)\,\omega_m e^{-\mu\theta}}{v_c}. \tag{5}$$

When the actuation is decoupled with the human, we assume that the necessary human ankle moment for achieving normal bipedal walking is generated entirely by the soleus. In this case

$$M_{\text{ankle}} = F_{\text{mu}} L_{\text{mu}} \tag{6}$$

where M_{ankle} represents the moment of the human ankle. F_{mu} represents the muscle force generated by the soleus, and L_{mu} symbolizes the moment arm of the muscle force relative to the center of rotation (CoR) of the ankle joint.

When the actuation provides concentric assistance for the humans, the necessary human ankle moment is generated partially by the actuation system. In this case

$$M_{\text{ankle}} = F'_{\text{mu}} L_{\text{mu}} + F_c L_{\text{exo}} \tag{7}$$

where F'_{mu} refers to the muscle force generated by the soleus under exoskeleton intervention, and L_{exo} refers to the moment arm of the cable force generated by the actuation system.

By combining (6) with (7), we can obtain

$$F'_{\text{mu}} = F_{\text{mu}} - \frac{F_c L_{\text{exo}}}{L_{\text{mu}}} < F_{\text{mu}}. \tag{8}$$

2) Eccentric Assistance: Oppositely, in the eccentric contraction period of the soleus (mainly in the midstance period of the human gait cycle), the mechanical clutch couples the pulley with the motor. The actuation will generate braking torque and exert passive moment on the human ankle as eccentric assistance to decrease ankle dorsiflexion acceleration and prevent ankle hyperflexion.

During this process, the pulley also rotates with the motor; thus, (1) still holds.

The torque generated by the actuation and exerted on the pulley can be expressed as (2).

According to the principle of power conservation, we can obtain

$$T_p\,(-\omega_p) = F_c\,(-v_c)\,\eta_B. \tag{9}$$

By combining (1), (2), (4), and (9), we can obtain the cable force

$$F_c = \frac{(T_m + T_s)\,\omega_m e^{-\mu\theta}}{v_c}. \tag{10}$$

Similar to the concentric assistance process, the necessary human ankle moment for achieving normal bipedal walking when the actuation is coupled or decoupled with the human can be expressed as

$$M_{\text{ankle}} = F_{\text{mu}} L_{\text{mu}} = F'_{\text{mu}} L_{\text{mu}} + F_c L_{\text{exo}}. \tag{11}$$

By combining (10) with (11), we can obtain

$$F'_{\text{mu}} = F_{\text{mu}} - \frac{F_c L_{\text{exo}}}{L_{\text{mu}}} < F_{\text{mu}}. \tag{12}$$

3) Transparent Mode: Furthermore, this actuation is designed according to the "assist-as-needed" principle, thus the transparent mode, which is a key requirement for assistive wearable robots [12], is also involved. In the swing phase of the human gait cycle, the ankle joint does not need to support the human body and the biomechanical ankle moment decreases substantially. Meanwhile, the ankle joint rotates freely to prepare for the next ground contact. The actuation is expected to exert minimized interaction force on the human in this period. And the interaction force between the wearable robot and the human is mainly generated by the torsion spring.

During this process, the motor stops next to the anticlockwise side edge of the end stop,

$$\omega_m = 0. \tag{13}$$

According to the principle of power conservation, we can obtain

$$T_s \omega_p = F_c v_c \eta_B. \tag{14}$$

By combining (4) with (14), we can obtain the cable force

$$F_c = \frac{T_s \omega_p e^{-\mu\theta}}{v_c}. \tag{15}$$

The interaction torque exerted on the ankle joint during dorsiflexion/plantarflexion is

$$M^r_{\text{ankle}} = F_c L_{\text{exo}} = \frac{T_s \omega_p L_{\text{exo}} e^{-\mu\theta}}{v_c}. \tag{16}$$

Above all, the proposed actuation is capable of cooperating with the human muscle and reducing muscle activation by applying proper assistive force to the muscle–tendon system theoretically, as described in (8) and (12). Moreover, the interaction torque between the device and the human is mainly generated by the pretensioned torsion spring in the transparent mode.

III. Control Strategy

In order to mimic the natural anisometric contractions of human muscles, a group of control strategies is designed for achieving corresponding assistive modes and mode switching. To be specific, a concentric assistance controller is conducted to aid the concentric contraction process of the human muscle while an eccentric assistance controller is implemented to supply assistance when the target human muscle is in eccentric contraction status. Besides, following the "assist-as-needed" principle, a mode switching controller, i.e., clutch engagement/disengagement controller, is also involved in the control architecture, for switching between assistive modes (concentric and eccentric assistance) and the transparent mode.

The electronics hardware of the control system consists of a two-layer control architecture: microprocessor (outer layer) and motor driver (inner layer). An ARM Cortex M7 processor (STMicroelectronics, Switzerland) is selected as the outer layer, in which the main controller is implemented. The main control

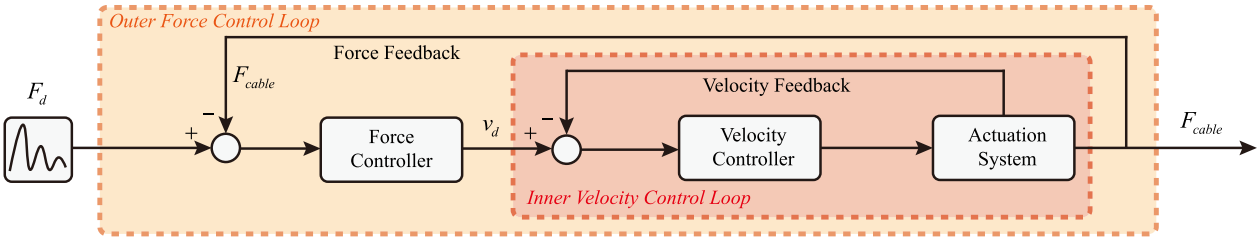

Fig. 3. Block diagram of the concentric assistance control. The force control loop is chosen as the outer layer of the concentric assistance controller, with the inner layer running a velocity control loop.

loop in the processor layer runs at 500 Hz. A motor driver (maximal voltage 75 V, rated current 20 A, YK-HS485, SpeedSmart Company, Ltd., China) is employed to interface with the motor and sensors including two magnetic encoders and a single-axis in-line load cell (FUTEK Advanced Sensor Technology, Inc., USA) for cable force measurements. The motor driver receives data from the motor encoder at 20 kHz, data from the pulley encoder at 1 kHz, and data from the load cell at 1 kHz. The processor layer communicates with the motor driver at 500 Hz.

A. Concentric Assistance Control

During the concentric contraction process of the human muscle, an active assistance force profile is expected to act on the human body in parallel with the muscle–tendon system. Hence, the force control loop is chosen as the outer layer of the concentric assistance controller, with the inner layer running a velocity control loop, as shown in Fig. 3. In the outer loop, the desired cable force profile is generated and sent to the proportional–integral force controller after subtracting the actual cable force measured by the load cell. The force control loop will iteratively generate and send the desired motor velocity command to the inner velocity control loop. Following the command from the force controller, the inner velocity controller will tune the motor speed correspondingly to accomplish proper active cable force output.

B. Eccentric Assistance Control

During the eccentric contraction process of the human muscle, the cable is unspooled from the pulley towed by the human. At this time, a resistance that hinders the cable movement is desired for absorbing the impact of human motion and reducing muscle activation. Following our previous works in prostheses [42], [43], a damping cable tension regulating method is implemented in this controller. Specifically, the motor is capable of behaving as a generator during passive rotation. According to the law of electromagnetic induction, an induced voltage E_a will be produced in the foregoing process. Furthermore, a resulting induced current I_a will be generated along the motor armature

$$I_a = \frac{E_a}{R_a} = \frac{C_E \phi n}{R_a} \tag{17}$$

where R_a represents the motor armature resistance, C_E, ϕ, and n refer to the electromotive constant, the magnetic field intensity, and the motor speed, respectively.

Then, the induced current will produce Ampere's force under the effect of the magnetic field and therewith the motor braking torque

$$\tau_b = C_T \phi I_a = \frac{C_T C_E \phi^2}{R_a} n = k_d n \tag{18}$$

where C_T is the motor torque constant, and k_d can be regarded as the damping coefficient.

Since the magnetic field intensity of the motor is hard to change in real time, we adjust the damping coefficient of the system by appropriately regulating the motor armature resistance R_a. The corresponding regulating circuits have been integrated into the motor driver.

C. Transparent Mode

In this design, the transparent mode is achieved by decoupling the cable with the geared motor; thus, the system transparency will not be affected by the back-drivability of the motor with reduction and fully depends on the pretension level of the torsion spring.

D. Mode Switching Control

The clutch is employed to switch between assistive modes and the transparent mode in this actuation. The mode switching celerity and accuracy mainly depend on the performance of the clutch status control. Following actual requirements in operation, the clutch engagement controller (switch from the transparent mode to assistive modes) and the clutch disengagement controller (switch from assistive modes to the transparent mode) are organized, respectively.

For clutch engagement control, the primary goal is to couple the pulley with the motor smoothly, since the mechanical collision and impact are unacceptable for robust control. On the premise of this, the engagement time is expected to be as short as possible. Generally, the pulley position profile θ_p can be treated as the desired position profile of the motor directly, in order to achieve the fastest contact. However, if the desired motor position is forthrightly commanded as the current pulley position, the motor may overshoot the desired position under the effect of inertia. Meanwhile, the driving block of the driving disc will collide with the driven block of the pulley. Hence, a position–velocity control loop is proposed as the outer layer to smooth the clutch engagement process, as depicted in Fig. 4(a). In this loop, the velocity of both the motor and the pulley is

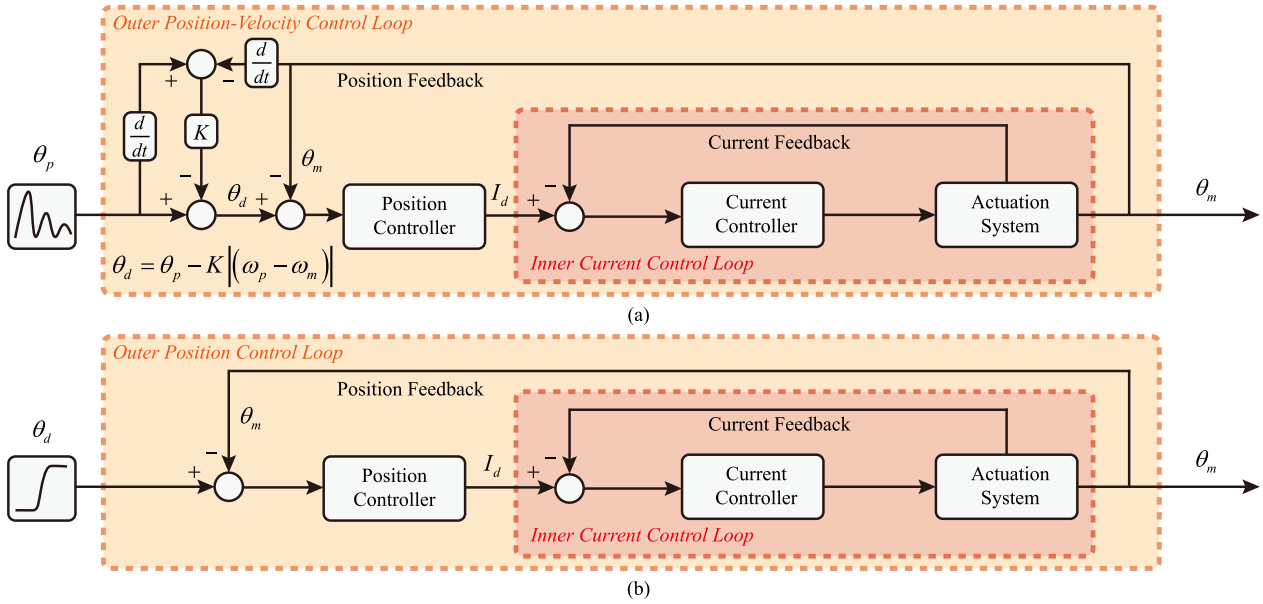

Fig. 4. Block diagram of the mode switching control. (a) Clutch engagement control refers to the mode switching control from the transparent mode to assistive modes. (b) Clutch disengagement control refers to the mode switching control from assistive modes to the transparent mode.

calculated in real time and utilized to modify the desired motor position profile,

$$\theta_d = \theta_p - K\left|(\omega_p - \omega_m)\right| \tag{19}$$

where θ_d and θ_p are the desired motor position and the actual pulley position, respectively. K refers to the amplifier. If $K \neq 0$, a position margin is reserved between the actual pulley position profile and the desired motor position profile. Furthermore, the margin size will shorten with the speed difference between the pulley and the motor decreasing. In this way, the motor position profile could encounter and coincide with the pulley position profile gradually and smoothly. In practice, the amplifier K needs to be regulated according to the actual application scenario.

For clutch disengagement control, the primary goal is to decouple the pulley from the motor as quickly as possible. In this case, a normal proportional–integral–differential position control loop is employed as the outer layer, with the inner layer running a current control loop, as illustrated in Fig. 4(b). The desired motor position θ_d is set as a point near the anticlockwise side edge of the end stop, to obtain the maximal free motion range of the cable.

IV. Actuation Performance Characterization

In order to comprehensively demonstrate the performance of the proposed actuation, a series of characterization experiments were conducted on a test bench, as shown in Fig. 5. The proposed actuation system was mounted on the left-hand side of the test bench while a towing system was fixed on the other side. The towing system was composed of a geared motor as same as the power source of the proposed actuation (SS-BLDC-6-300,

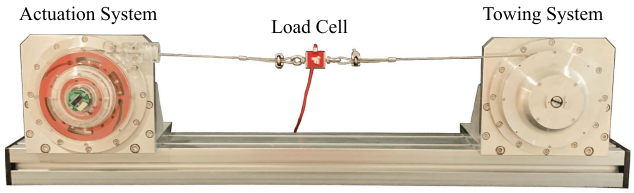

Fig. 5. Test bench setup. The pulley of the actuation system mounted on the left-hand side can be pulled clockwise rotate by the towing system fixed on the other side of the test bench and return to its initial position under the effect of the torsion spring when the cable is released by the towing system. The pulley of the towing system can be fixed firmly on the frame of the test bench.

SpeedSmart Company, Ltd., China), a 43.5-mm radius single-wrap pulley, a motor encoder (EBI-1135, Heidenhain, Germany), and a motor driver (G-TW125/100SRS, Elmo Motion Control, Ltd., Israel). The pulley of the towing system is capable of being fixed firmly on the frame of the test bench alternatively. A steel cable with an in-line load cell links the pulley of the proposed actuation with that of the towing system. The data of encoders and the data of the load cell are collected with a frequency of 500 Hz.

A. Concentric Assistance Control

To reveal the active force-tracking performance of the proposed actuation in the concentric assistance control, we conducted bandwidth test experiments by commanding sinusoidal sweep force signals (from 1 Hz to 20 Hz) with a magnitude of 50 N (peak to peak 100 N), and 75 N (peak to peak 150 N), respectively. The testing parameters were selected according to the assistance magnitudes of related soft exoskeletons and the actual bandwidths of the proposed actuation system. In these tests, the pulley of the towing system was fixed firmly on the

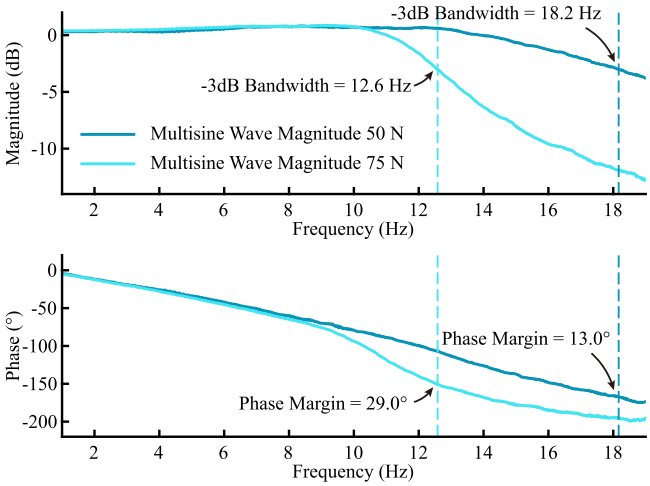

Fig. 6. Bandwidth test results of the concentric assistance control. Bandwidth was calculated as the lesser of the -3 dB cutoff frequency and the -180° phase offset crossover frequency.

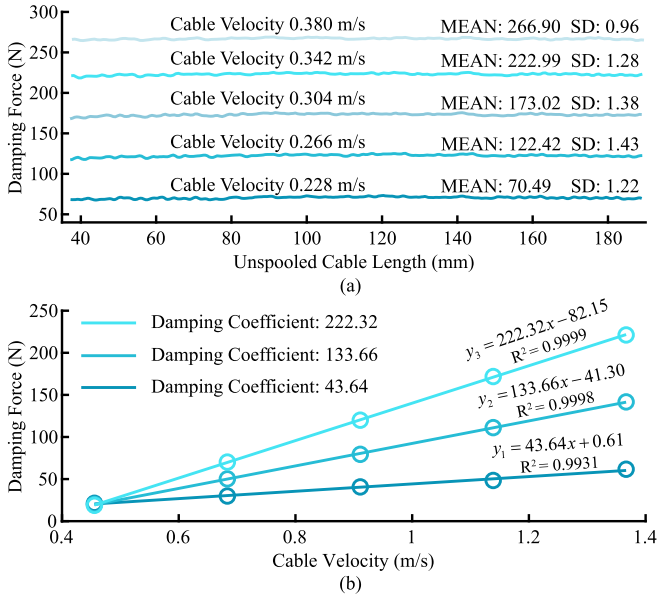

Fig. 7. Damping test results of the eccentric assistance control. (a) Actuation with a preset damping parameter was pulled to rotate passively by the towing system in a series of constant speeds. (b) Three groups of damping control with different fitting coefficients were conducted by regulating the set damping parameter.

frame of the test bench, i.e., the cable output of the proposed actuation was stuck. Under each magnitude, 10 rounds of tests were performed repetitively.

The desired and measured force signals of the same round were fed to the Fourier transformation. Then, the frequency domain data of magnitude and phase were retrieved. After averaging over 10 rounds in the frequency domain, the Bode plots of the actuation with force controller were obtained, as shown in Fig. 6. Bandwidth was calculated as the lesser of the -3 dB cutoff frequency and the -180° phase offset crossover frequency. The gain-limited closed-loop bandwidths of the system with 50-N and 75-N magnitude were 18.2 Hz with a phase margin of 13.0° and 12.6 Hz with a phase margin of 29.0°, respectively.

B. Eccentric Assistance Control

To verify the effectiveness of the proposed eccentric assistance control, the damping cable tension generated by the actuation system was evaluated in two experimental conditions, as illustrated in Fig. 7. At first, the actuation was pulled to rotate passively by the towing system in a series of constant speeds (cable velocity: 0.228 m/s, 0.266 m/s, 0.304 m/s, 0.342 m/s, and 0.380 m/s). And the cable tension generated by the actuation with fixed damping parameter changed slightly during the whole process [see Fig. 7(a)]. To be specific, the standard deviations (SDs) of the force data generated during motion were 1.22 N, 1.43 N, 1.38 N, 1.28 N, and 0.96 N, respectively, corresponding to the five cable velocities. Then, three groups of damping control with different fitting coefficients were conducted by regulating the set damping parameter [see Fig. 7(b)]. The fitting coefficients of the three groups were 43.64 (with an *R*-squared value of 0.9931), 133.66 (with an *R*-squared value of 0.9998), and 222.32 (with an *R*-squared value of 0.9999), respectively.

Besides, to investigate the power efficiency of the damping tension regulating method employed in this study compared with the common active motor braking method, two groups of comparative experiments were conducted as well. In these experiments, ensuring the same cable motion input, the actuation was commanded to output similar cable force profiles by means of damping tension regulating and active motor braking (current control), respectively.

As shown in Fig. 8, in the damping tension regulating experiment, connecting a diode in series between the motor driver and the power supply so as to allow the current only flow from the power supply to the motor driver. In this case, if the power generated by the motor (working as a generator) exceeds the working power consumption of the motor driver, the excess energy will be stored in capacitors, which will increase the capacitor voltage, i.e. the power supply voltage. When the capacitor voltage is higher than 48 V, there will be no current output from the power supply, and the driver is completely powered by the energy collected by capacitors. Therefore, the energy collection can be reflected by the change of capacitor voltage. The capacitors utilized in this experiment include 24 electrolytic capacitors connected in parallel, with a total capacitance of

$$C = 4700 \times 10^{-6} \times 20 + 300 \times 10^{-6} \times 4 = 0.0952 \text{ F}. \tag{20}$$

In the damping tension regulating experiment, the average power collected by capacitors can be calculated by

$$\overline{P_d} = \frac{C\left(U_2^2 - U_1^2\right)}{2\tilde{}T} = 19.8 \text{ W} \tag{21}$$

where the positive value presents power generation, U_2 refers to the terminating voltage, U_1 refers to the initial voltage, and T refers to the time duration.

In the active motor braking experiment, the average power consumption of the mechatronic system can be described as the

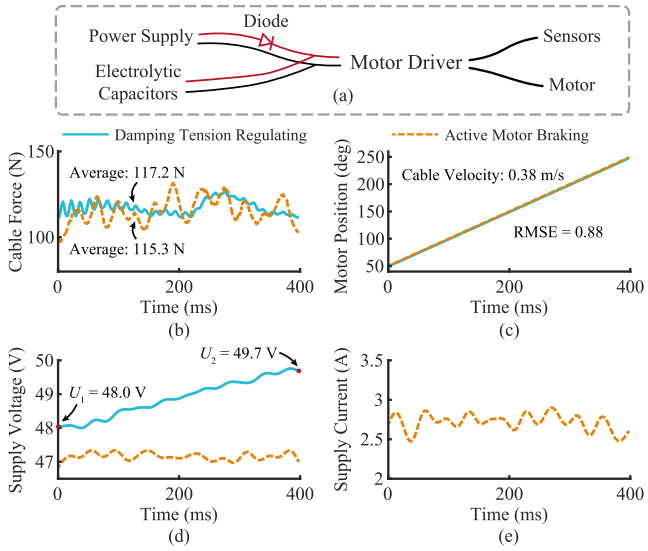

Fig. 8. Power efficiency comparison results. In the damping tension regulating experiment, the actuation performed the damping control employed in this study. In the active motor braking experiment, the actuation performed current control. The solid blue lines present profiles under damping tension regulation, and the dashed orange lines present profiles under active motor braking. (a) Experimental setup. (b) Output cable force profiles. (c) Motor position profiles. (d) Supply voltage profiles. (e) Supply current profiles of active motor braking. Raw supply voltage and supply current signals were filtered using zero-lag eighth-order low-pass Butterworth filters with 30-Hz cut-off frequencies.

product of supply voltage U_a and supply current I_a

$$\overline{P_a} = -\overline{(U_a I_a)} = -128.2 \text{ W} \tag{22}$$

where the negative value presents power consumption.

The power efficiency of the damping tension regulating method employed in this study compared with the common active motor braking method is defined as ΔP

$$\Delta P = \overline{P_d} - \overline{P_a} = 148 \text{ W}. \tag{23}$$

C. Transparent Mode

Transparency is an important index to evaluate the performance of the system when assistance is not needed. A transparency evaluation experiment was performed on the aforementioned test bench. In this experiment, the cable with the pulley of the proposed actuation was towed by the towing system to move passively back and forth with the magnitude of 100 mm (peak to peak 200 mm), since the maximum free motion range of the cable was about 250 mm (demonstrated in Section II) and bidirectional position margins were reserved to prevent the mechanical collision. The frequency of the commanding sinusoidal position input signals generated by the towing system ranged from 0.5 Hz to 2.5 Hz, since 2.5 Hz is sufficient to supply assistance for bipedal walking with normal speeds and is the highest frequency of input position signal, which the towing system can provide in such magnitude. The cable force data, i.e., the system resistance of the proposed actuation was captured by the in-line load cell during the towing process. The raw force data was filtered using zero-lag 8th-order low-pass Butterworth filters with 20-Hz cut-off frequencies. As described

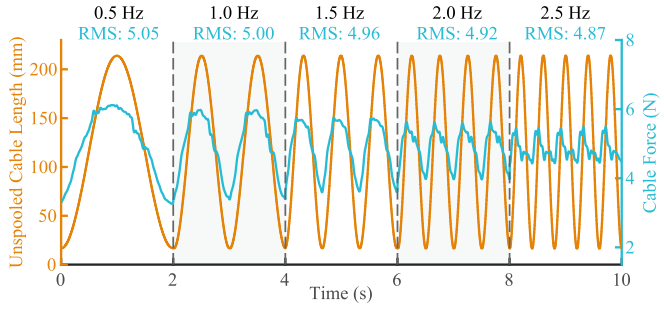

Fig. 9. System resistance test results of the transparent mode. rms: The root mean square of the cable force. The oscillation amplitude of the cable force profile decayed gradually with the frequency of the input sinusoidal signal increasing while the rms also decreased slightly with the frequency going up.

in Fig. 9, the oscillation amplitude of the cable force profile decayed gradually with the frequency of the input sinusoidal signal increasing. Meanwhile, the root mean square (rms) of the cable force data also decreased slightly with frequency going up (5.05 N at 0.5 Hz, 5.00 N at 1.0 Hz, 4.96 N at 1.5 Hz, 4.92 N at 2.0 Hz, and 4.87 N at 2.5 Hz).

D. Mode Switching Control

The controller employed to achieve the mode switch from assistive modes to the transparent mode (clutch disengagement) in this actuation is a normal proportional–integral–differential position controller. Ten rounds of bandwidth test experiments were performed to evaluate the position-tracking performance of the actuation with clutch disengagement control. We conducted these experiments by commanding sinusoidal sweep position signals (from 10 Hz to 50 Hz) with the magnitude of 10° (peak to peak 20°) as the desired motor position profile. Due to the mechanical feature of the proposed clutch, once a small angular position gap was reserved between the driving block of the driving disc and the driven block of the pulley, the clutch disengagement process could be considered complete. Furthermore, 20° was big enough for the angular position gap and, thus, was selected as the testing amplitude. Besides, the frequency sweeping range of 10–50 Hz was selected to illustrate the bandwidth of the proposed actuation system completely. After Fourier transformation, the frequency domain data of magnitude and phase were retrieved. As depicted in Fig. 10, the Bode plots were obtained by averaging the frequency-domain data over 10 rounds. Bandwidth was also calculated as the lesser of the -3 dB cutoff frequency and the $-180°$ phase offset crossover frequency. The gain-limited closed-loop bandwidth of the system was 40.4 Hz with a phase margin of 101.5°.

Besides, the performance of the mode switching control from the transparent mode to assistive modes (clutch engagement control) was characterized in the time domain. Four groups of evaluation experiments including twelve rounds were performed overall. For the first three groups of evaluation experiments, similarly, the cable and the pulley of the proposed actuation were towed by the towing system to move passively back and forth. The frequencies of the commanding sinusoidal position input signals generated by the towing system were 0.5 Hz [see

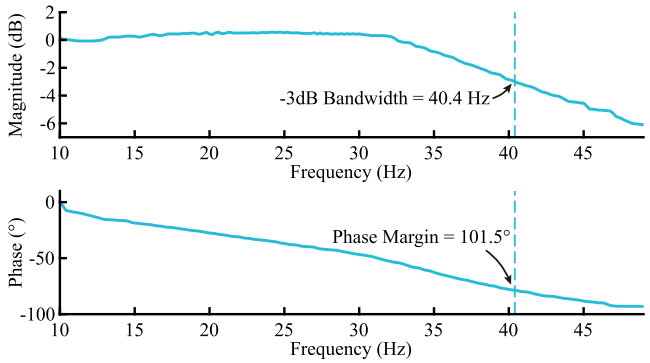

Fig. 10. Bandwidth test results of the clutch disengagement control. Bandwidth was calculated as the lesser of the -3 dB cutoff frequency and the -180° phase offset crossover frequency.

Fig. 11(a)], 1.0 Hz [see Fig. 11(b)], and 1.5 Hz [see Fig. 11(c)], respectively. For the last group of tests, the cable and the pulley of the actuation were towed by the human hand to simulate an application scenario with a frequency of about 2.0 Hz [see Fig. 11(d)].

In these evaluation experiments, the proposed actuation was commanded to accomplish clutch engagement near (before, when, and after) the maximal unspooled cable length was achieved. When the angular distance between the driving block of the driving disc and the driven block of the pulley was less than 5°, the clutch engagement control process was over, and the motor was commanded to track the pulley position profile back and forth in real time. To prevent the free movement of the pulley from being hindered by the motor, a position margin was reserved between the actual pulley position profile and the commanded motor position profile in the position tracking control. The contact force ratio (CFR) was proposed to evaluate the system resistance or collision induced by the motor quantitatively

$$\mathrm{CFR} = \frac{F_{\text{control}}^{\max} - F_{\text{free}}^{\max}}{F_{\text{free}}^{\max}} \times 100\% \tag{24}$$

where $F_{\text{free}}^{\max}$ refers to the maximal cable force during the motor decoupling with the pulley completely, $F_{\text{control}}^{\max}$ refers to the maximal cable force during the motor interfering with the pulley. As illustrated in Fig. 11, the mean(SD) engagement time of the clutch control was 91.17(20.97) ms, and the CFR induced by the motor was 5.01(4.71)% over the 12 rounds of evaluation experiments.

V. Wearable Robot Application

To evaluate the performance of the proposed actuation system in an actual scenario, a soft ankle exoskeleton was developed as the testing platform (see Fig. 12). Similar to the existing devices [14], [44], the testing ankle exoskeleton consists of a calf cuff with a sheath attachment, a custom shoe with a cable attachment, and a pressure insole with two pressure transducers under the human toe and heel, respectively. The proposed actuation system is arranged remotely to provide mechanical power for the exoskeleton. The sheath of the Bowden cable links the actuation with the sheath attachment on the calf cuff, and the inner cable with an in-line load cell (FUTEK Advanced Sensor Technology, Inc., USA) is attached to the cable attachment behind the custom shoe. The exoskeleton applies the assistive force in parallel with the soleus–Achilles-tendon system of the human.

A 12-camera marker-based motion capture system was employed to collect the kinematics information of the human ankle joint. The pressure insole was utilized to detect the key events (heel strike, toe strike, heel off, and toe off) in the human gait cycle. During level-ground walking on an instrumented treadmill (Gaitway-3D 150/50, h/p/cosmos & Arsalis, Germany & Belgium), the actuation system acts in different modes according to the real-time gait phase of the wearer. To be specific, between the heel strike and the toe strike, the actuation is commanded to accomplish clutch engagement. After the toe strike, the actuation will follow the eccentric assistance control to aid the soleus–Achilles-tendon system in preventing the ankle joint from rotating too fast and ensuring the body weight moves forward smoothly until the heel off is detected. And then, the actuation will provide concentric assistance during the push-off period. Once the toe off is detected, the actuation will be commanded to achieve clutch disengagement. A single-peak force profile is generated during the push-off period, according to

$$F_d(t) = \begin{cases} F_{\text{in}} + (F_p - F_{\text{in}}) \cdot \sin\left(\frac{\pi t}{T}\right), & 0 \le t < \frac{T}{2} \\ F_p \cdot \sin\left(\frac{\pi t}{T}\right), & \frac{T}{2} \le t < T \end{cases} \tag{25}$$

where T refers to the assistive cycle length while F_d, F_{in}, and F_p define the desired assistive force, initial cable force, and peak force magnitude, respectively. In practice, F_{in} is recorded by the load cell at the end of the eccentric assistance control while F_p and T are preset parameters.

A. Experimental Protocol

1) Subject: A healthy subject (male, 24 years old, 1.78 m, 77 kg) was recruited in the application experiments. The study was approved by the local ethics committee of Peking University, and the participant was given informed written consent prior to participation.

2) Experimental Design: To describe the functionalities of the proposed actuation system, two independent experiments were conducted in total.

Trial 1 (Unassisted level-ground walking): At first, a group of unassisted level-ground walking experiments including three independent rounds were performed to quantify the system resistance of the ankle exoskeleton. The subject wearing the unpowered exoskeleton in clutch disengagement status walked on the treadmill for a minute at different speeds. Three walking speeds (0.8 m/s, 1.0 m/s, and 1.2 m/s) were selected for the three rounds, respectively. In these experiments, the kinematic information of the human ankle and the cable force measured by the load cell were recorded and stored.

Trial 2 (Assisted level-ground walking): After the processes above, the actuation system was powered ON, and the exoskeleton supplied corresponding assistance for the subject. Then, a group of level-ground walking experiments including three independent rounds with three different speeds (0.8 m/s, 1.0 m/s,

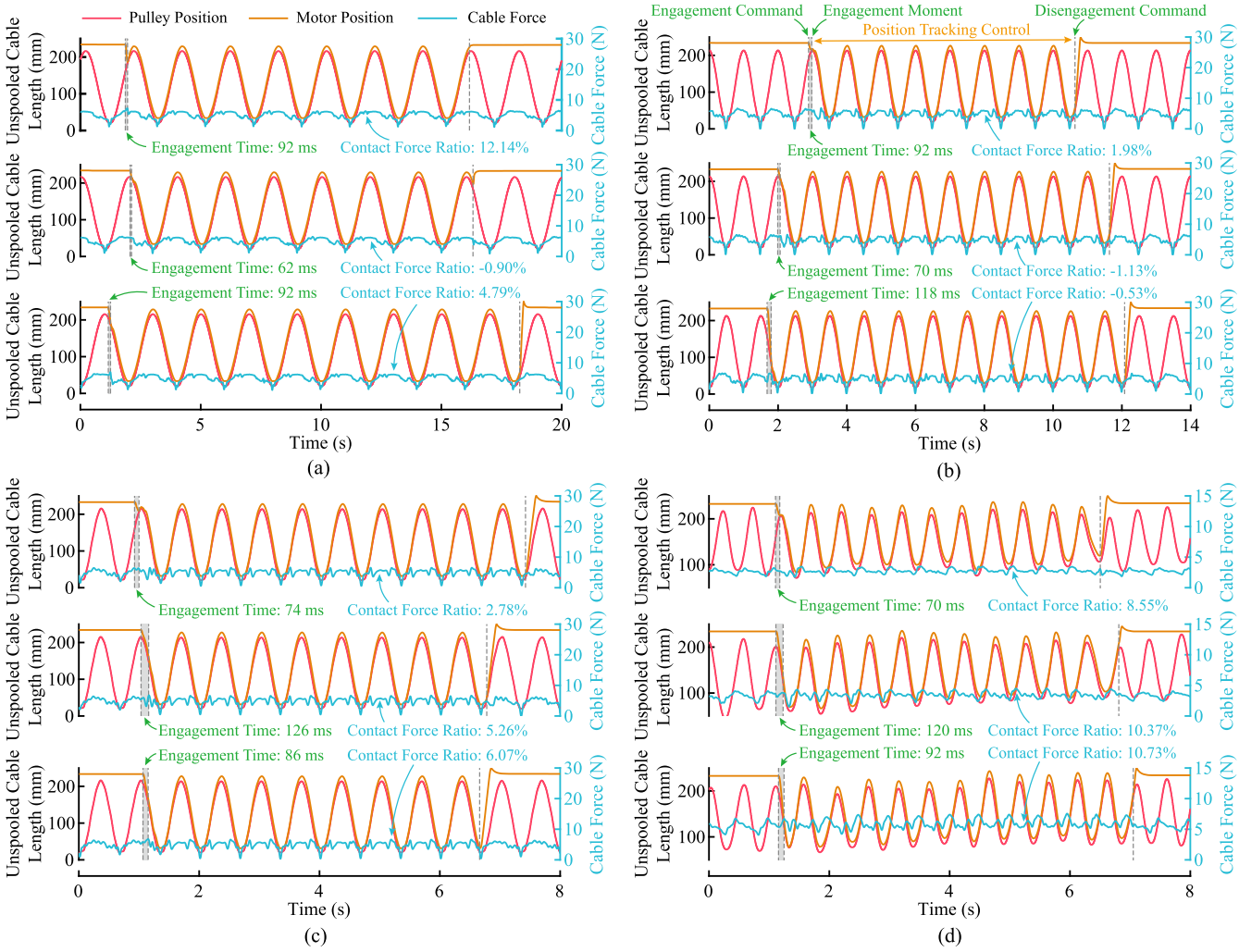

Fig. 11. Results of the mode switching control conducted on the test bench. The motor position refers to the driving disc position, i.e., the output position of the geared motor. The proposed actuation was commanded to accomplish clutch engagement near (before, when, and after) the maximal unspooled cable length was achieved. After the clutch engagement, the driving disc rotated with the pulley of the actuation back and forth following the position tracking control, until receiving the disengagement command. (a) The frequency of the sinusoidal signal: 0.5 Hz. (b) The frequency of the sinusoidal signal: 1.0 Hz. (c) The frequency of the sinusoidal signal: 1.5 Hz. (d) The frequency of the sinusoidal signal: about 2.0 Hz.

and 1.2 m/s) were conducted to evaluate the actual performance of the proposed actuation. The subject wearing the powered exoskeleton walked on the treadmill for a minute in each round. In these experiments, the kinematic information of the human ankle and the actuation-related data were recorded and stored.

B. Data Acquisition and Processing

The data from the motor encoder, pulley encoder, load cell, and pressure insole were synchronously collected by the main controlling hardware of the actuation system and stored in a personal computer with a sampling frequency of 500 Hz. The raw force data captured by the load cell was filtered using zero-lag eighth-order low-pass Butterworth filters with 20-Hz cut-off frequencies. The captured kinematic data of six reflective markers were collected and stored in another personal computer with a sampling frequency of 100 Hz. All the data were synchronously collected through a trigger signal.

C. Walking Evaluations

In order to ensure that the results were computed from steady-state walking data, only the middle 10-s data including several consecutive gait cycles were taken from every 1-min walk for further demonstration, as depicted in Figs. 13 and 14. During unassisted level-ground walking with 0.8 m/s, 1.0 m/s, and 1.2 m/s (*Trial 1*), as shown in Fig. 14, the maximum system resistances detected by the load cell were 12.60 N, 12.68 N, and 15.15 N, respectively.

The assisted level-ground walking data (*Trial 2*) involving the human ankle angle, the motion status of the pulley and motor, and the cable force was visualized in Fig. 13. And the quantitative evaluations shown in Fig. 15 were computed from the force data of Fig. 13. The control processes and experimental results in *Trial 2* were described as follows.

After the heel strike, the actuation was commanded to accomplish clutch engagement. In this process, the motor (driving disc) did not collide with the pulley, and a little position margin

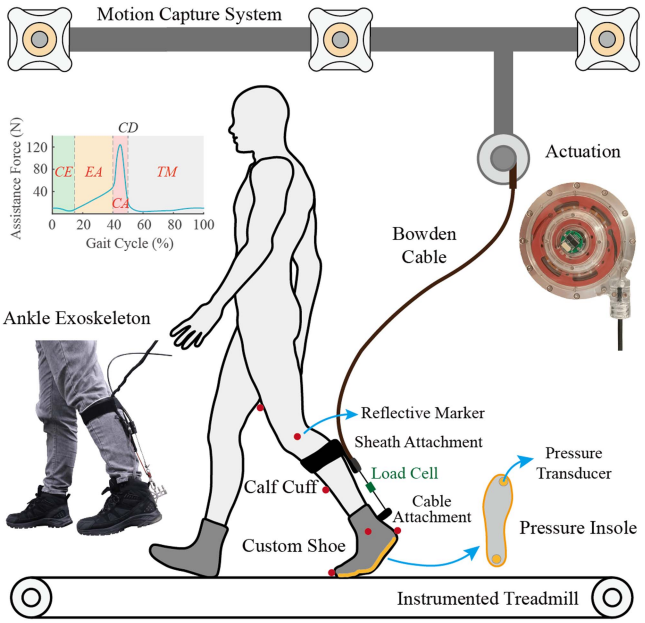

Fig. 12. Overview of the wearable robot application test environment. Similar to the existing devices [14], [44], the testing ankle exoskeleton consists of a calf cuff with a sheath attachment, a custom shoe with a cable attachment, and a pressure insole with two pressure transducers under the human toe and heel, respectively. In this figure, CE refers to the clutch engagement, CD refers to the clutch disengagement, EA refers to the eccentric assistance, CA refers to the concentric assistance, and TM refers to the transparent mode.

was reserved between them (see the position profiles in Fig. 13). Furthermore, the cable force was equivalent to the system resistance in this period. The mean(SD) of the maximal cable forces in the clutch engagement process over the three walking speeds was 11.77(0.77) N while the mean(SD) of rms was 7.46(0.36) N, as illustrated in Fig. 15(a).

After the toe strike, the little position margin was eliminated by the wearer, and then, the actuation following the eccentric control rotated passively pulled by the wear (see the position profiles in Fig. 13). In this process, a damping cable force for assisting the eccentric contraction of the soleus was applied to the subject. And the mean(SD) of the maximal damping forces over the three walking speeds was 44.44(1.69) N while the mean(SD) of rms was 30.97(1.25) N. As illustrated in Fig. 15(c), the MAX and rms of the damping force generated by the actuation increased with walking speed. To be specific, compared to walking with 0.8 m/s, the MAX of damping force during walking with 1.0 m/s and 1.2 m/s increased by 2.02% and 7.59% while the rms increased by 7.21% and 7.42%, respectively.

Once the heel off was detected, the actuation system would be commanded to supply concentric assistance. In this process, a single-peak force profile was generated as the desired cable force profile according to (25). Three indexes including peak value, peak time, and rms of the cable force were employed to evaluate the force tracking performance in practice. Compared with peak values of desired cable force profiles, that of actual cable force profiles exhibited slight divergences (+1.16% for 0.8 m/s, +0.17% for 1.0 m/s, -1.10% for 1.2 m/s), as shown in Fig. 15(d). In terms of peak time, the actual cable force profiles reached their maximums later (8.99% for 0.8 m/s, and 2.22% for 1.0 m/s) or earlier (9.23% for 1.2 m/s) than the corresponding desired cable force profiles, as illustrated in Fig. 15(e). Besides, as depicted in Fig. 15(f), the rms of actual cable force profiles were lower than that of desired cable force profiles (6.57% for 0.8 m/s, 6.01% for 1.0 m/s, and 6.06% for 1.2 m/s), because of the initial decrease process of actual cable force profile, which resulted by the motor status switching delay between passive mode and active mode.

After the toe off was detected, the actuation system would follow the clutch disengagement control, and the exoskeleton would exhibit the transparent mode. In this period, the captured cable force was equivalent to the system resistance. To be specific, as shown in Figs. 15(b) and 14, during walking with 0.8 m/s, 1.0 m/s, and 1.2 m/s, the maximal cable forces in transparent mode (or unassisted walking) were 12.51 N (12.60 N), 12.98 N (12.68 N), and 15.24 N (15.15 N), respectively. The mean(SD) of the maximal cable forces over the three walking speeds was 13.58(1.46) N while the mean(SD) of rms was 9.59(0.64) N. Overall, the proposed actuation system was capable of supplying assistance as commanded stably.

VI. Evaluation Experiments

A. Experimental Protocol

To quantitatively assess the effects of the proposed design, several groups of surface EMG measurement experiments were conducted in this section. Generally, the soleus performs eccentric contraction during each stride to decelerate ankle dorsiflexion after foot strikes in normal locomotion [8]. During level-ground and uphill walking, the duration and magnitude of soleus eccentric contraction are relatively small while great efforts are made by concentric contraction for forward propulsion and energy generation [45], [46], [47]. By contrast, additional eccentric muscle contraction is performed by the soleus of the human to lower the center of mass and achieve energy absorption in downhill walking, and the activation level of concentric contraction decreases accordingly [45], [48], [49]. Hereby, for emphasizing the contribution of eccentric contraction in bipedal ambulation to some extent, downhill walking was selected as the test scenario.

In these EMG measurement experiments, the soft ankle exoskeleton powered by the proposed actuation system (see Fig. 12) was evaluated on five able-bodied subjects (male, 24.00 $\pm$ 1.41 years old, 1.80 $\pm$ 0.05 m, 75.80 $\pm$ 7.39 kg) walking downhill on an instrumented treadmill at 1.0 m/s under three conditions: 1) normal walking without the exoskeleton (without exo), 2) walking with the unpowered exoskeleton (assist off), and 3) walking with the powered exoskeleton (assist on). None of the participants reported having any known or apparent injuries that could affect their gait. Under each condition, participants walked on the treadmill for 6 min, with the first 3 min for training and the second for data collection. Two trials of independent EMG measurement experiments were performed in total, including downhill walking on 8° declination (*Trial 1*) and 5° declination (*Trial 2*). The study was approved by the local ethics committee

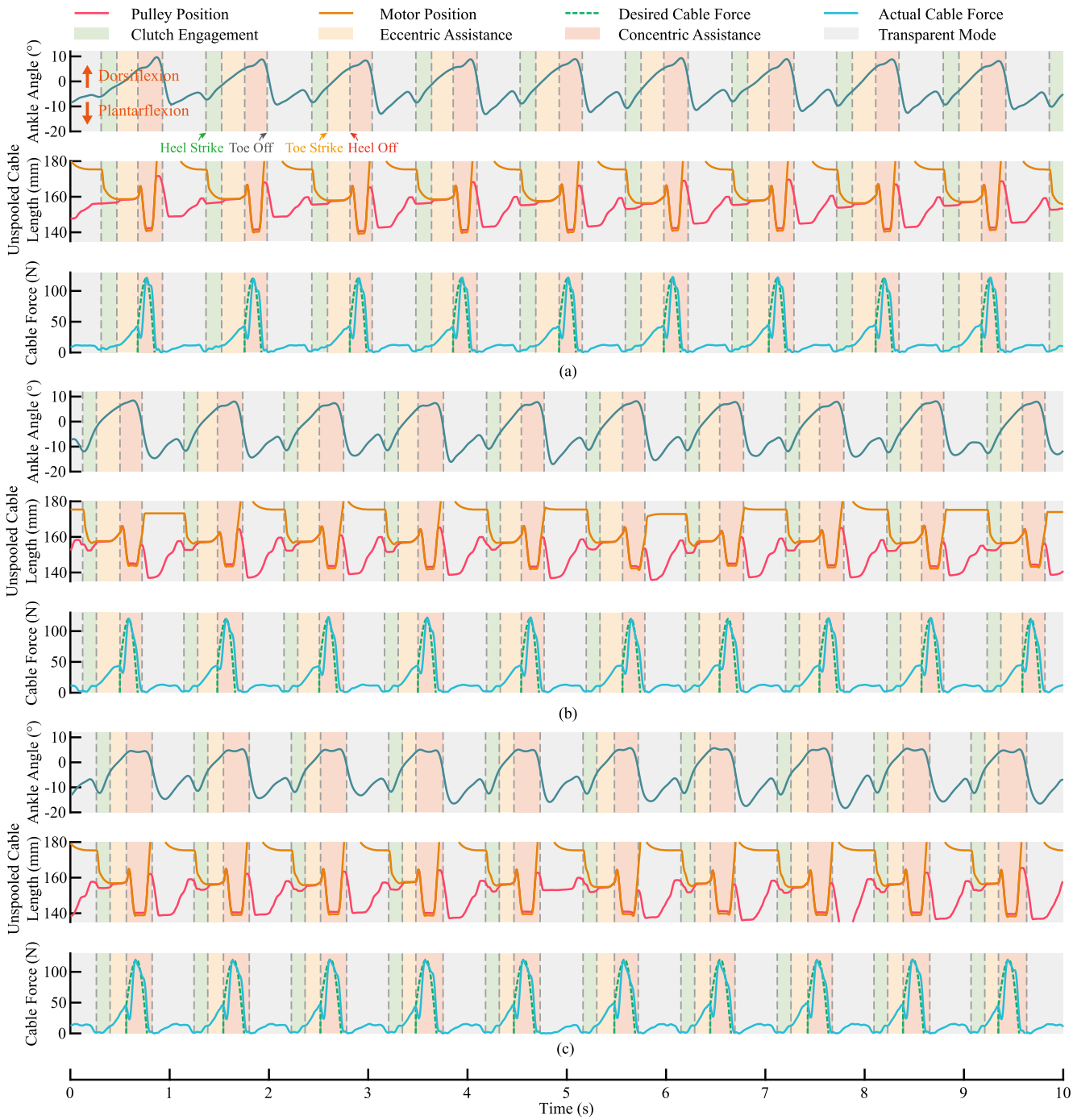

Fig. 13. Results of assisted level-ground walking in several consecutive gait cycles. The motor position refers to the driving disc position, i.e., the output position of the geared motor. The actuation was controlled to supply corresponding assistance according to the gait phase of the subject. (a) Assisted level-ground walking with 0.8 m/s. (b) Assisted level-ground walking with 1.0 m/s. (c) Assisted level-ground walking with 1.2 m/s.

of Peking University, and the participant was given informed written consent prior to participation.

During all trials, surface EMG signals from four calf muscles of subjects were recorded at 1 kHz by means of a wireless system (Trigno Wireless EMG System, Delsys, USA). Muscles investigated in this study were soleus (SOL), tibialis anterior (TA), medial gastrocnemius (MG), and lateral gastrocnemius (LG), respectively. Prior to EMG electrode fixation, the skin surface was shaved and cleaned with alcohol. And electrodes were placed following SENIAM guidelines. Three-dimensional ground reaction forces were measured at 1 kHz using an instrumented treadmill. The exoskeleton-related data, EMG signals, and ground reaction forces were collected simultaneously with the motion data measured by the motion capture system.

Raw EMG signals were high-pass filtered with a cutoff frequency of 20 Hz, rectified and low-pass filtered with a cutoff frequency of 6 Hz to create muscle-activity linear envelopes, similar to the work in [30]. For each participant and each muscle,

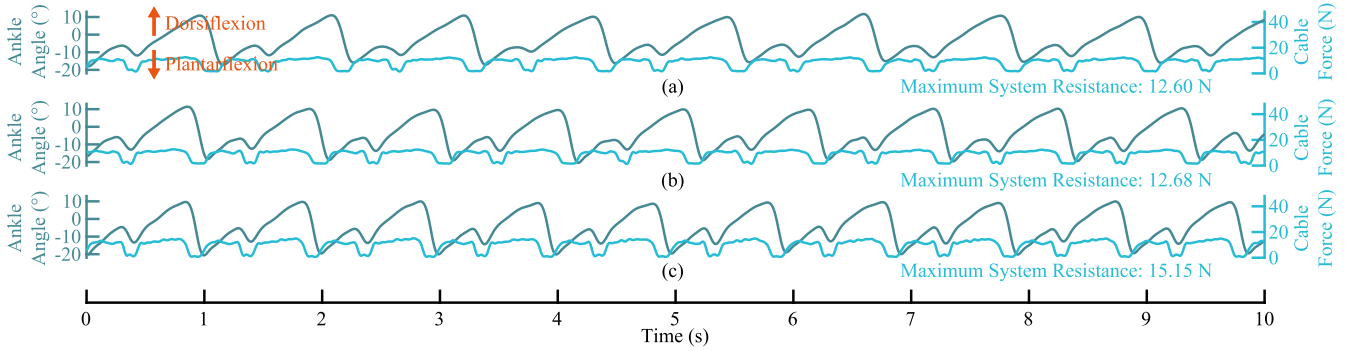

Fig. 14. System resistance test results of unassisted level-ground walking in several consecutive gait cycles. During unassisted level-ground walking with 0.8 m/s, 1.0 m/s, and 1.2 m/s (*Trial 1*), the maximum system resistances detected by the load cell were 12.60 N, 12.68 N, and 15.15 N, respectively. (a) Unassisted level-ground walking with 0.8 m/s. (b) Unassisted level-ground walking with 1.0 m/s. (c) Unassisted level-ground walking with 1.2 m/s.

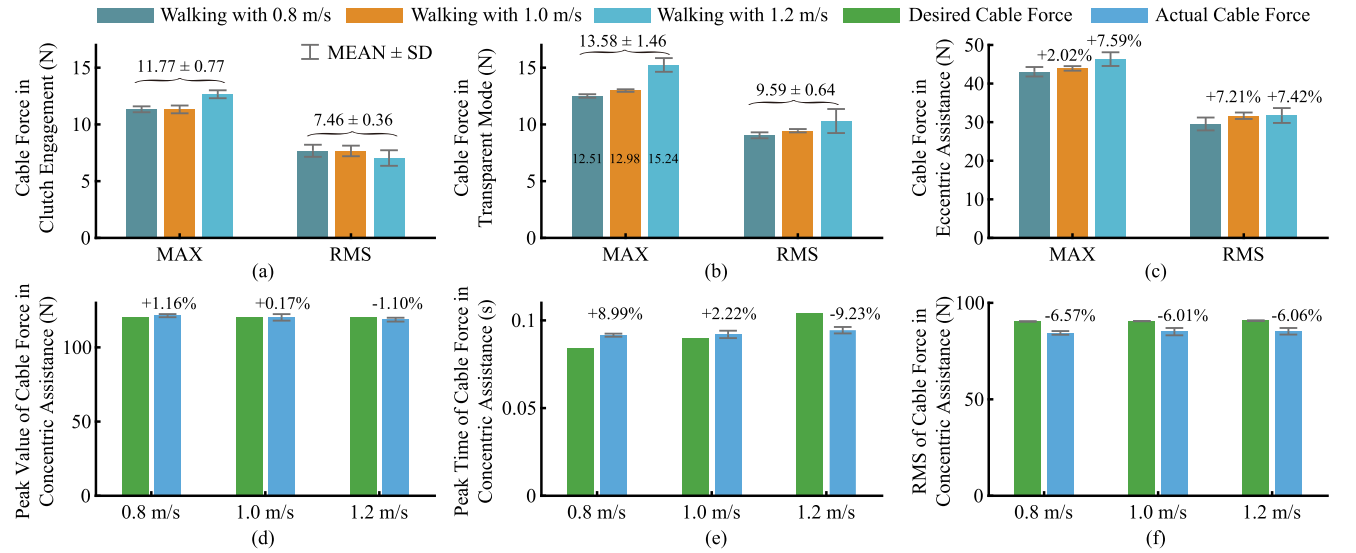

Fig. 15. Quantitative evaluations for assisted level-ground walking. The results shown in this figure were computed from the force data of Fig. 13. The MAX and rms represent the peak value and root mean square of cable force during the specific period, respectively. (a)–(c) Comparison of evaluation indexes for cable force profiles under the three walking speeds in the clutch engagement period, transparent period, and eccentric assistance period, respectively. (d)–(f) Comparison between the desired cable force profiles and the actual cable force profiles under the three walking speeds in terms of peak value, peak time, and rms, respectively.

the resulting EMG linear envelope was then normalized by the maximum activation (averaged across twenty consecutive strides) recorded during the normal walking condition (without exo).

All results from each walking session were separated into gait cycles using ground reaction force data and normalized to each gait cycle. A gait cycle was considered to be the period between subsequent heel strikes of the left leg [20]. For each walking session, 20 consecutive strides from steady-state walking data were used to compute averages and then plot comparisons between conditions.

To quantitatively evaluate the changes in muscle activities, rms values were calculated from the averaged EMG curves of each walking session. Then, the rms values of the assist-on condition and the assist-off condition were compared with the value of the without-exo condition to compute the rates of change for each muscle activity. Finally, the rates of change for each muscle activity across five subjects were averaged and analyzed statistically.

One-way analysis of variance (ANOVA) was used to compare changes among different experimental conditions (in all statistical analyses, the significant level $\alpha = 0.05$), and the least significant difference post-hoc analysis was performed to determine which differences were significant among conditions.

B. EMG Measurement Results

Fig. 16 presents a representative comparison of average muscle activities of SOL [see Fig. 16(c)], TA [see Fig. 16(d)], MG [see Fig. 16(e)], and LG [see Fig. 16(f)] over the whole stride during downhill walking on 8° declination under the three conditions (*Trial 1*). The measured muscle activities were reduced under the assist-on condition compared with the assist-off condition and the without-exo condition during the eccentric and concentric assistance period. TA activity increased during the swing phase under the assist-off and assist-on conditions, due to the system resistance introduced by the pretensioned torsion spring.

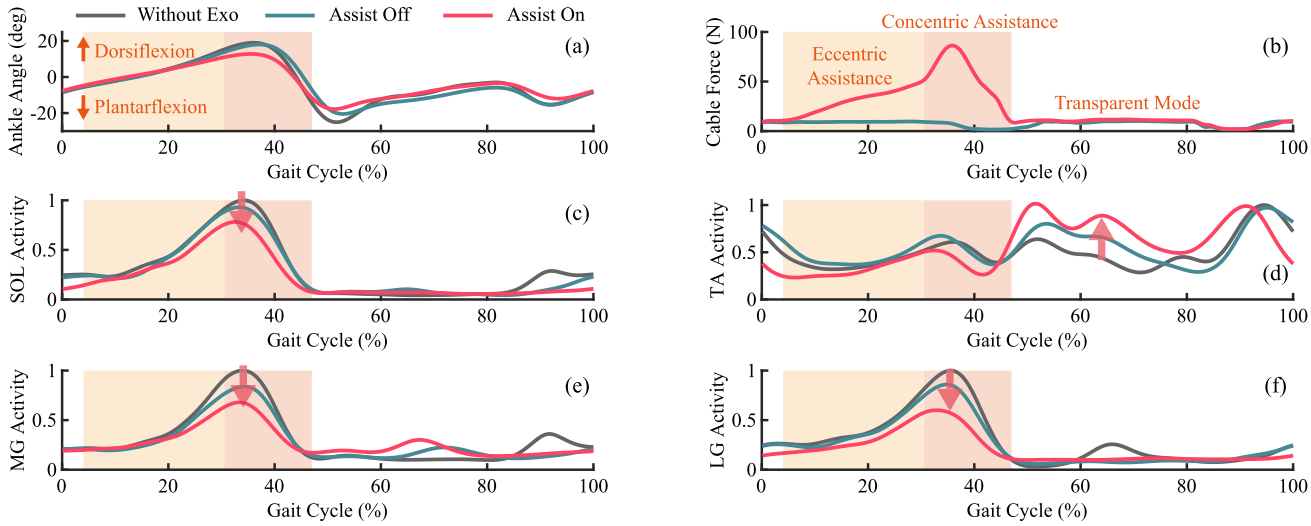

Fig. 16. Representative comparison of dynamic results during downhill walking on 8° declination under each condition (*Trial 1*, Subject AB01). The curves represent the three different conditions: 1) Without exo (gray), 2) assist off (green), and 3) assist on (red). (a) Average ankle angle profiles as a percent of the gait cycle. (b) Average cable force profiles as a percent of the gait cycle. (c)–(f) Normalized EMG linear envelope as a percent of the gait cycle for the four muscles examined: 1) Soleus (SOL), 2) TA, 3) MG, and 4) LG.

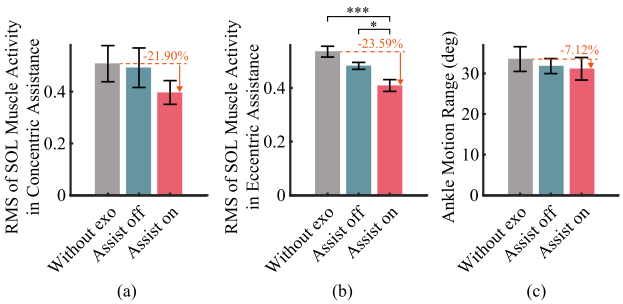

Fig. 17. Changes of soleus muscle activities in the assistance period and ankle motion ranges in the whole stride ($N = 5$, Mean ± S.E.M) under the assist-on condition and assist-off condition compared with normal walking (without exo) in *Trial 1*. (a) Changes of soleus muscle activity rms in the concentric assistance period. (b) Changes of soleus muscle activity rms in the eccentric assistance period. (c) Changes of ankle motion range in the whole stride. *: $p < 0.05$; **: $p < 0.01$; ***: $p < 0.001$.

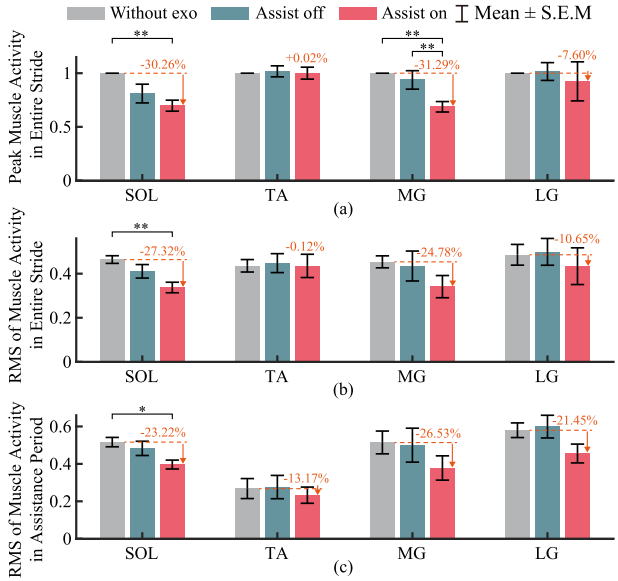

Fig. 18. Changes of muscle activities ($N = 5$) under the assist-on condition and the assist-off condition compared with normal walking (without exo) in *Trial 1*. (a) Changes of peak muscle activity in the entire stride. (b) Changes of muscle activity rms in the entire stride. (c) Changes of muscle activity rms in the assistance period. *: $p < 0.05$; **: $p < 0.01$; ***: $p < 0.001$.

To evaluate muscle activities statistically across all subjects, Fig. 17 shows the changes of SOL muscle activities over the assistance period and ankle motion ranges over the whole stride (*Trial 1*) while Fig. 18 presents the changes of EMG activities on all measured muscles (*Trial 1*).

Significant reductions were observed in EMG activities of SOL under the assist-on condition compared with walking without exo. To be specific, the reduction was 23.59% for muscle activity rms over the eccentric assistance period ($p = 0.0005$), 30.26% for peak muscle activity over the entire stride ($p = 0.0032$), 27.32% for muscle activity rms over the entire stride ($p = 0.0033$), and 23.22% for muscle activity rms over the assistance period ($p = 0.0145$), respectively. Moreover, for muscle activity rms over the eccentric assistance period, the reduction was 21.90% but no significant difference was found.

Reduction trends were also observed in EMG activities of the gastrocnemius (MG and LG) in terms of the three indexes employed, as shown in Fig. 18. In particular, significantly lower peak muscle activation (31.29%) was reported in the MG ($p = 0.0022$). Over the whole stride, the peak activation and muscle activity rms of TA remained virtually unchanged. In the assistance period, the rms of TA activity was reduced by 13.17%. However, no significant difference was found in the changes of TA activities. Besides, the average ankle motion range was reduced by 7.12% under intervention without a significant difference being found.

Fig. 19 shows a representative comparison of average muscle activities over the whole stride during downhill walking on 5°

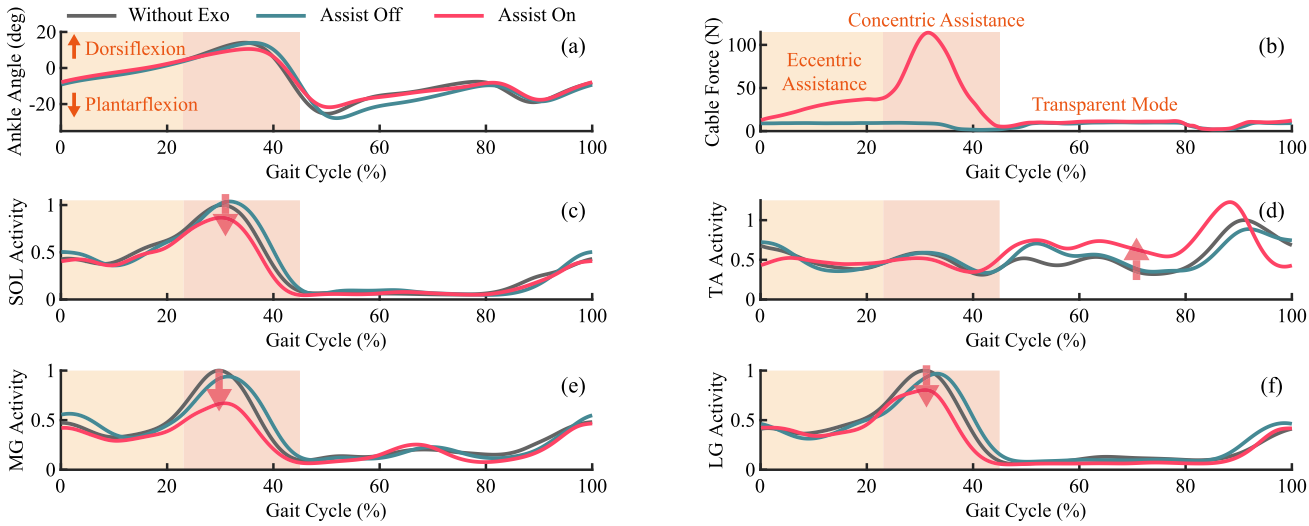

Fig. 19. Representative comparison of dynamic results during downhill walking on 5° declination under each condition (*Trial 2*, Subject AB01). The curves represent the three different conditions: 1) Without exo (gray), 2) assist off (green), and 3) assist on (red). (a) Average ankle angle profiles as a percent of the gait cycle. (b) Average cable force profiles as a percent of the gait cycle. (c)–(f) Normalized EMG linear envelope as a percent of the gait cycle for the four muscles examined: 1) Soleus (SOL), 2) TA, 3) MG, 4) and LG.

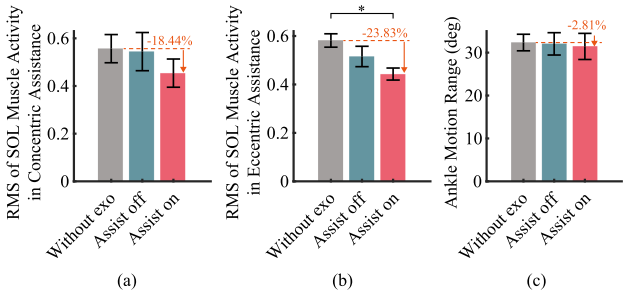

Fig. 20. Changes of soleus muscle activities in the assistance period and ankle motion ranges in the whole stride ($N = 5$, Mean ± S.E.M) under the assist-on condition and the assist-off condition compared with normal walking (without exo) in *Trial 2*. (a) Changes of soleus muscle activity rms in the concentric assistance period. (b) Changes of soleus muscle activity rms in the eccentric assistance period. (c) Changes of ankle motion ranges in the whole stride. *: $p < 0.05$; **: $p < 0.01$; ***: $p < 0.001$.

declination under the three conditions (*Trial 2*). In this trial, similar changes were also observed across all the investigated muscles. During the eccentric and concentric assistance period, the measured muscle activities were reduced compared with normal walking. In the swing phase, TA activity increased because of the spring force.

Figs. 20 and 21 present the changes of muscle activities across all the subjects statistically (*Trial 2*). Significant reductions were observed in EMG activities of SOL under the assist-on condition compared with the without exo condition. To be specific, the reduction was 23.83% for muscle activity rms over the eccentric assistance period ($p = 0.0106$), 19.29% for peak muscle activity over the entire stride ($p = 0.0396$), 21.30% for muscle activity rms over the entire stride ($p = 0.0352$), and 21.54% for muscle activity rms over the assistance period ($p = 0.0495$), respectively. Moreover, for muscle activity rms over the eccentric assistance period, the reduction was 18.44%, but no significant difference was found.

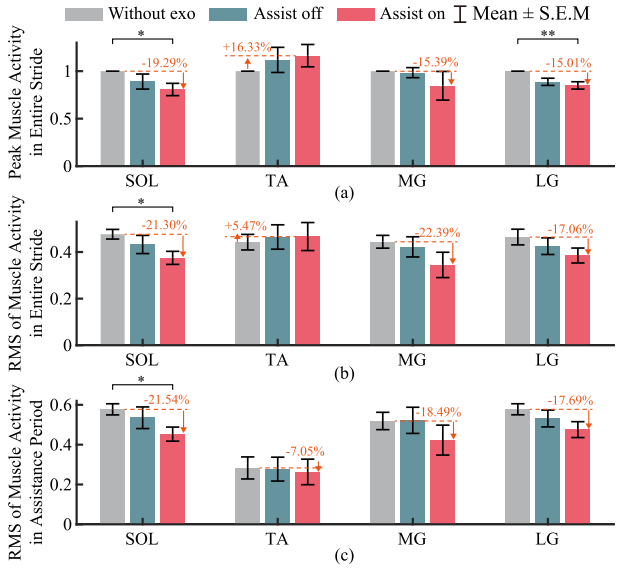

Fig. 21. Changes of muscle activities ($N = 5$) under the assist-on condition and the assist-off condition compared with normal walking (without exo) in *Trial 2*. (a) Changes of peak muscle activity in the entire stride. (b) Changes of muscle activity rms in the entire stride. (c) Changes of muscle activity rms in the assistance period. *: $p < 0.05$; **: $p < 0.01$; ***: $p < 0.001$.

Reduction trends were also observed in EMG activities of the gastrocnemius (MG and LG) in terms of the three indexes employed, as shown in Fig. 21. In particular, significantly lower peak muscle activation (15.01%) was reported in the LG ($p = 0.0053$). Over the whole stride, the peak activation and muscle activity rms of TA increased by 16.33% and 5.47%, respectively. In the assistance period, the rms of TA activity was reduced by 7.05%. However, no significant difference was found in the changes of TA activities. Besides, the average ankle motion range was reduced by 2.81% under intervention without a significant difference being found.

TABLE I
COMPARISON WITH RELATED STUDIES IN TERMS OF ACTUATION FUNCTIONALITY AND IMPLEMENTATION METHODS

Study	Concentric Assistance	Eccentric Assistance	Transparent Mode	Mode Switching
[14, 15, 30, 31]	Active motor rotation	Active motor rotation	Cable slack management	Motor rotation control
[28, 29]	Active motor rotation	Active motor rotation	"Zero-torque" control	Motor rotation control
[27]	Active motor rotation	Active motor braking	–	Motor rotation control
[13]	Spring contraction	Spring elongation	Clutch disengagement	Passive clutch
[20]	–	Controllable mechanical load	–	–
[35–37]	–	–	Clutch disengagement	Active clutch (Extra power source)
This study	Active motor rotation	Damping tension regulation	Clutch disengagement	Active clutch (Motor rotation control)

VII. DISCUSSION

In this study, a bioinspired cable-driven actuation system capable of providing anisometric contractions assistance or nearly acting as a transparent device is presented. Comparison with related studies in terms of actuation functionality and implementation methods is illustrated in Table I. Compared with existing designs, the advantages and drawbacks of the proposed actuation are analyzed and summarized as follows.

A. Advantages of Bioinspired Actuation System

1) Efficient Eccentric Assistance: In the state of the art, most powered cable-driven exoskeletons/orthoses are capable of supplying both eccentric and concentric assistance by actuating the driving motor actively [14], [15], [28], [29], [30], [31]. However, it is not efficient to assist eccentric contraction by commanding the motor to rotate actively according to the human joint angle [14], [15], [28], [29], [30], [31], since plenty of extra electrical power will be consumed in this process. In addition, although the eccentric assistance force was passively generated by the natural ankle dorsiflexion in [27], commanding the motor to stay at a fixed position was also with nonignorable electrical energy consumption. Unlike these devices, following our previous works in prostheses [42], [43], a damping cable tension regulating method was designed for the proposed actuation. Compared with active motor braking, supplying eccentric assistance with generator status is an energy-saving and environment-friendly method [43]. To be specific, when cable force output was about 115 N, applying the damping tension regulating method was capable of collecting electric power by 19.8 W while 128.2 W needs to be consumed for active motor braking, as illustrated in Section IV-B.

2) Sufficient Concentric Assistance: In terms of concentric assistance control, to the best of our knowledge, the gain-limited closed-loop bandwidths for the systems proposed in [31] and [30] were 19.6 Hz (with a 45-mm radius pulley and a cable magnitude of 100 N, after feedforward optimization) and 13.0 Hz (with a 10-mm radius pulley and a cable magnitude of 160 N), respectively. By contrast, the gain-limited closed-loop bandwidths for the proposed actuation were 18.2 Hz and 12.6 Hz, with the magnitude of commanding sinusoidal sweep force signal being 50 N and 75 N (peak to peak 150 N, with a 43.5-mm radius pulley), respectively. Although the system bandwidths were slightly lower than them [30], [31], it is still sufficient for human movement assistance. To be specific, for the harmonic movement of the human, the highest frequency is below 6 Hz [8]. And for bipedal walking with normal speeds (0.8–1.2 m/s), the movement frequency of the human lower limb only ranges from 1.0 Hz to 1.5 Hz [45]. Besides, due to the motor status switching delay between passive mode and active mode (about 10 ms), the actual assistive level in level-ground walking experiments is slightly lower than the commanded level, as shown in Figs. 13 and 15(d).

3) Reliable System Transparency: The transparency of the proposed actuation is achieved by decoupling the pulley with the driving motor and, thus, is not affected by the back-drivability of the motor with reduction. After clutch disengagement, the remaining human–robot interaction force mainly generated by the torsion spring is utilized to keep the cable in tension. And the transparency of the system entirely depends on the pretensioned level of the torsion spring. Although complete system transparency could be achieved by cable slack management [14], [15], [30], [31], pushing the cable out to slack during the nonassistive phase will lead to cable derailment from the pulley due to the transmission friction. Furthermore, the derailment may cause the cable to jam between the pulley and the case, resulting in unexpected system failure [32]. Keeping the cable in tension is meaningful to avoid cable derailment and make the transmission more compliant [38]. Moreover, the torsion spring is capable of cooperating with the motor to supply assistance force in assistive modes. Although the spring force acts as system resistance in some phases of the human motion cycle, the elastic energy converted from the kinetic energy of the human will be released to aid the human in other phases eventually, except the energy dissipation caused by the system friction, according to the conservation of energy. Besides, compared with the "zero-torque" control [28], [29], the system transparency achieved in this way did not worsen with the frequency of human harmonic movement increasing [33], [34], as demonstrated in Section IV-C.

4) Simpler Mode Switching: For the mode switches between assistive modes and transparent mode, the switching process

TABLE II
PERFORMANCE COMPARISON WITH RELATED STUDIES FOR REDUCING SOLEUS MUSCLE ACTIVATION

Author	Type	Index	Baseline	Change of Soleus Activity
Collins et al. [13]	Passive	Average	Without exo	22% reduction (midstance period)
Wang et al. [50]	Quasi-passive	rms	Without exo	6.8% reduction
Panizzolo et al. [51]	Active	Average	Assist off	8.4% reduction
Ding et al. [52]	Active	rms	Assist off	About 4% reduction
Chen et al. [30]	Active	rms	Without exo	24.4% reduction under single-motor assistance
Wang et al. [53]	Active	rms	Without exo	11.98% reduction
Durandau et al. [54]	Active	rms	Assist off	20.5% reduction
Tan et al. [55]	Active	rms	Assist off	11% reduction
This study	Active	rms	Without exo	27.32% reduction (over stride) 23.59% reduction (midstance period)
This study	Active	Average	Without exo	26.42% reduction (over stride) 25.28% reduction (midstance period)

of the proposed actuation mainly depends on a unidirectional mechanical clutch, which is controlled by the driving motor in common with cable slack management and "zero-torque" control. To the best of our knowledge, there is no clutch being employed to accomplish the foregoing mode switches in powered cable-driven exoskeletons/orthoses without rigid structures. Compared with the conventional decoupling method utilized in rigid exoskeletons, i.e., employing electromechanical/magnetic clutch [35], [36], [37], the proposed actuation is very compact and does not introduce another power source apart from the driving motor. In terms of engagement time, the electromagnetic tooth type clutch adopted in [35] was 37 ± 2 ms while the electromechanical friction-based clutches employed in [36] and [37] were 36.2 ± 2 ms and about 60 ms, respectively. The engagement time of the proposed clutch (about 90 ms) meets the actual requirements in common activities of human daily living, even though it is not as short as that of conventional clutches. To be specific, the proposed clutch was capable of coupling/decoupling the pulley with the motor as expected during level-ground walking with 1.2 m/s, as shown in Fig. 13. Furthermore, traditional tooth type or friction-based clutches could also be applied to the proposed actuation easily, without regard to system weight or power source simplicity.

5) Effective EMG Reduction: Applying the proposed actuation system to power the ankle exoskeleton, calf muscle activation was significantly reduced, particularly in the soleus, as demonstrated in Section VI. The performance comparison with related studies for reducing soleus muscle activation is illustrated in Table II. To the best of our knowledge, in group studies, only the ankle exoskeleton proposed in [30] established comparable results in reducing soleus muscle activation. It was noteworthy that the study [30] reduced soleus muscle activation by 24.4% with the actuation output torque of 30 N · m (under single-motor assistance), and 32.5% with the actuation output torque of 50 N · m (under dual-motor assistance). By contrast, employing the bioinspired actuation system mentioned in our study established similar soleus muscle activation reduction by 27.32%, with only an obviously smaller output torque of 10 N · m.

B. Limitations and Future Work

In this article, we focus on putting forward a general actuation design idea for most cable-driven wearable robots supplying unidirectional assistance. A prototype design was implemented in an efficient manner. The performance characterization results verified its feasibility in supplying human motion assistance, though some improvements and optimizations should be conducted in the future.

The limitations of this study are described as follows. For one thing, the synergy mechanisms between the proposed design and the human muscle were analyzed qualitatively without quantitative evaluation being conducted, since it is hard to measure the soleus muscle contraction force from the triceps surae muscle group directly. Instead, surface EMG signals from five healthy subjects were measured and analyzed to address this issue. For another, the controllers employed in walking experiments could not adapt to different walking speeds and walking cadences after control parameter regulation. Besides, in the test bench evaluations, the cable was not covered by the outer sheath for the mounting of the in-line load cell; thus, extra frictional and damping factors may be introduced into walking experiments after the outer sheath installation.

In further research, more subjects will be involved in the validations, and other gaits on different terrains could be included. Future works of this study may also include the following directions. The torsion spring could be customized to exactly counteract the friction generated in transmission. Moreover, the feed-forward friction compensation model could be adopted into the control architecture. The controllers employed in the walking experiments could be developed into adaptive controllers. The

electrical power generated during eccentric assistance could be collected by the battery and utilized to power the actuation.

VIII. Conclusion

In this article, we proposed a bioinspired actuation design that can be directly applied to most cable-driven exoskeletons providing unidirectional assistance. The actuation was capable of supplying concentric and eccentric assistance according to the activation status of human muscles, or nearly acting as a transparent device when assistance is not needed. The eccentric assistance was provided through damping cable tension regulation, a more efficient way compared with actuating the motor actively. And the system transparency was achieved by decoupling the cable pulley with the driving motor. The mode switches between assistive modes and the transparent mode fully depends on a unidirectional mechanical clutch controlled by the driving motor. Corresponding control strategies were designed to coordinate with the proposed mechanical design. Both performance evaluations conducted on a test bench and walking experiments with EMG measurements performed on an ankle exoskeleton revealed that the proposed actuation was capable of supplying assistance as commanded stably and effectively and showed its application potential in existing wearable robotic devices.

Acknowledgment

The authors would like to thank the anonymous reviewers for their valuable suggestions. The authors would also like to thank T. Zhang, G. Zhang, and Y. Zhou for their support in circuits and mechanical structures. They would like to thank Dr. Jiang for his valuable suggestions and also thank X. Wu, Z. Wang, R. Wang, W. Zhu, and Q. Feng for their assistance in experiments.

References

[1] A. M. Dollar and H. Herr, "Lower extremity exoskeletons and active orthoses: Challenges and state-of-the-art," *IEEE Trans. Robot.*, vol. 24, no. 1, pp. 144–158, Feb. 2008.

[2] A. T. Asbeck, S. M. D. Rossi, I. Galiana, Y. Ding, and C. J. Walsh, "Stronger, smarter, softer: Next-generation wearable robots," *IEEE Robot. Autom. Mag.*, vol. 21, no. 4, pp. 22–33, Dec. 2014.

[3] A. J. Young and D. P. Ferris, "State of the art and future directions for lower limb robotic exoskeletons," *IEEE Trans. Neural Syst. Rehabil. Eng.*, vol. 25, no. 2, pp. 171–182, Feb. 2017.

[4] M. Xiloyannis et al., "Soft robotic suits: State of the art, core technologies, and open challenges," *IEEE Trans. Robot.*, vol. 38, no. 3, pp. 1343–1362, Jun. 2022.

[5] R. Cauchi, K. P. Camilleri, M. A. Saliba, and J. Attard, "Isometric and anisometric contraction relationships with surface electromyography," in *Proc. IEEE 43rd Annu. Int. Conf. Eng. Med. Biol. Soc.*, 2021, pp. 6368–6371.

[6] F. E. Zajac, R. R. Neptune, and S. A. Kautz, "Biomechanics and muscle coordination of human walking: Part I: Introduction to concepts, power transfer, dynamics and simulations," *Gait Posture*, vol. 16, no. 3, pp. 215–232, 2002.

[7] P. Madeleine, P. Bajaj, K. Søgaard, and L. Arendt-Nielsen, "Mechanomyography and electromyography force relationships during concentric, isometric and eccentric contractions," *J. Electromyogr. Kinesiol.*, vol. 11, no. 2, pp. 113–121, 2001.

[8] D. A. Winter, *Biomechanics and Motor Control of Human Movement*. Hoboken, NJ, USA: Wiley, 2009.

[9] K. Nishikawa, "Eccentric contraction: Unraveling mechanisms of force enhancement and energy conservation," *J. Exp. Biol.*, vol. 219, no. 2, pp. 189–196, 2016.

[10] R. Riener, M. Rabuffetti, and C. Frigo, "Stair ascent and descent at different inclinations," *Gait Posture*, vol. 15, no. 1, pp. 32–44, 2002.

[11] B. S. Davidson, D. L. Judd, A. C. Thomas, R. L. Mizner, D. G. Eckhoff, and J. E. Stevens-Lapsley, "Muscle activation and coactivation during five-time-sit-to-stand movement in patients undergoing total knee arthroplasty," *J. Electromyogr. Kinesiol.*, vol. 23, no. 6, pp. 1485–1493, 2013.

[12] Y. Zhang, K. J. Nolan, and D. Zanotto, "Oscillator-based transparent control of an active/semiactive ankle-foot orthosis," *IEEE Robot. Automat. Lett.*, vol. 4, no. 2, pp. 247–253, Apr. 2019.

[13] S. H. Collins, M. B. Wiggin, and G. S. Sawicki, "Reducing the energy cost of human walking using an unpowered exoskeleton," *Nature*, vol. 522, no. 7555, pp. 212–215, 2015.

[14] B. T. Quinlivan et al., "Assistance magnitude versus metabolic cost reductions for a tethered multiarticular soft exosuit," *Sci. Robot.*, vol. 2, no. 2, 2017, Art. no. eaah4416.

[15] P. Slade, M. J. Kochenderfer, S. L. Delp, and S. H. Collins, "Personalizing exoskeleton assistance while walking in the real world," *Nature*, vol. 610, no. 7931, pp. 277–282, 2022.

[16] C. Khazoom, C. Véronneau, J.-P. L. Bigué, J. Grenier, A. Girard, and J.-S. Plante, "Design and control of a multifunctional ankle exoskeleton powered by magnetorheological actuators to assist walking, jumping, and landing," *IEEE Robot. Autom. Lett.*, vol. 4, no. 3, pp. 3083–3090, Jul. 2019.

[17] T. Boaventura and J. Buchli, "Acceleration-based transparency control framework for wearable robots," in *Proc. IEEE/RSJ Int. Conf. Intell. Robots Syst.*, 2016, pp. 5683–5688.

[18] S. Bastide, N. Vignais, F. Geffard, and B. Berret, "Interacting with a "transparent" upper-limb exoskeleton: A human motor control approach," in *Proc. IEEE/RSJ Int. Conf. Intell. Robots Syst.*, 2018, pp. 4661–4666.

[19] J. Kim et al., "Reducing the metabolic rate of walking and running with a versatile, portable exosuit," *Science*, vol. 365, no. 6454, pp. 668–672, 2019.

[20] M. Shepertycky, S. Burton, A. Dickson, Y.-F. Liu, and Q. Li, "Removing energy with an exoskeleton reduces the metabolic cost of walking," *Science*, vol. 372, no. 6545, pp. 957–960, 2021.

[21] N. Vitiello et al., "NEUROExos: A powered elbow exoskeleton for physical rehabilitation," *IEEE Trans. Robot.*, vol. 29, no. 1, pp. 220–235, Feb. 2013.

[22] Y. Mao and S. K. Agrawal, "Design of a cable-driven arm exoskeleton (CAREX) for neural rehabilitation," *IEEE Trans. Robot.*, vol. 28, no. 4, pp. 922–931, Aug. 2012.

[23] T. Chen, R. Casas, and P. S. Lum, "An elbow exoskeleton for upper limb rehabilitation with series elastic actuator and cable-driven differential," *IEEE Trans. Robot.*, vol. 35, no. 6, pp. 1464–1474, Dec. 2019.

[24] S.-W. Pu, Y.-C. Pei, and J.-Y. Chang, "Decoupling finger joint motion in an exoskeletal hand: A design for robot-assisted rehabilitation," *IEEE Trans. Ind. Electron.*, vol. 67, no. 1, pp. 686–697, Jan. 2020.

[25] J.-Y. Kuan, K. A. Pasch, and H. M. Herr, "A high-performance cable-drive module for the development of wearable devices," *IEEE/ASME Trans. Mechatron.*, vol. 23, no. 3, pp. 1238–1248, Jun. 2018.

[26] B. K. Dinh, M. Xiloyannis, L. Cappello, C. W. Antuvan, S.-C. Yen, and L. Masia, "Adaptive backlash compensation in upper limb soft wearable exoskeletons," *Robot. Auton. Syst.*, vol. 92, pp. 173–186, 2017.

[27] D. G. Schmitz et al., "Modulation of Achilles tendon force with load carriage and exosuit assistance," *Sci. Robot.*, vol. 7, no. 71, 2022, Art. no. eabq1514.

[28] E. J. Park et al., "A hinge-free, non-restrictive, lightweight tethered exosuit for knee extension assistance during walking," *IEEE Trans. Med. Robot. Bionics*, vol. 2, no. 2, pp. 165–175, May 2020.

[29] K. Schmidt et al., "The Myosuit: Bi-articular anti-gravity exosuit that reduces hip extensor activity in sitting transfers," *Front. Neurorobot.*, vol. 11, 2017, Art. no. 57.

[30] J. Chen, J. Han, and J. Zhang, "Design and evaluation of a mobile ankle exoskeleton with switchable actuation configurations," *IEEE/ASME Trans. Mechatron.*, vol. 27, no. 4, pp. 1846–1853, Aug. 2022.

[31] G. Lee, Y. Ding, I. G. Bujanda, N. Karavas, Y. M. Zhou, and C. J. Walsh, "Improved assistive profile tracking of soft exosuits for walking and jogging with off-board actuation," in *Proc. IEEE/RSJ Int. Conf. Intell. Robots Syst.*, 2017, pp. 1699–1706.

[32] H. In, U. Jeong, H. Lee, and K.-J. Cho, "A novel slack-enabling tendon drive that improves efficiency, size, and safety in soft wearable robots," *IEEE/ASME Trans. Mechatron.*, vol. 22, no. 1, pp. 59–70, Feb. 2017.

[33] M. K. Shepherd and E. J. Rouse, "Design and validation of a torque-controllable knee exoskeleton for sit-to-stand assistance," *IEEE/ASME Trans. Mechatron.*, vol. 22, no. 4, pp. 1695–1704, Aug. 2017.

[34] X. Liu, Z. Zhou, J. Mai, and Q. Wang, "Real-time mode recognition based assistive torque control of bionic knee exoskeleton for sit-to-stand and stand-to-sit transitions," *Robot. Auton. Syst.*, vol. 119, pp. 209–220, 2019.
[35] T. Zhang and H. Huang, "Design and control of a series elastic actuator with clutch for hip exoskeleton for precise assistive magnitude and timing control and improved mechanical safety," *IEEE/ASME Trans. Mechatron.*, vol. 24, no. 5, pp. 2215–2226, Oct. 2019.
[36] M. R. Tucker, C. Shirota, O. Lambercy, J. S. Sulzer, and R. Gassert, "Design and characterization of an exoskeleton for perturbing the knee during gait," *IEEE Trans. Biomed. Eng.*, vol. 64, no. 10, pp. 2331–2343, Oct. 2017.
[37] K. Shamaei, M. Cenciarini, A. A. Adams, K. N. Gregorczyk, J. M. Schiffman, and A. M. Dollar, "Design and evaluation of a quasi-passive knee exoskeleton for investigation of motor adaptation in lower extremity joints," *IEEE Trans. Biomed. Eng.*, vol. 61, no. 6, pp. 1809–1821, Jun. 2014.
[38] J. Dittli, U. A. Hofmann, T. Bützer, G. Smit, O. Lambercy, and R. Gassert, "Remote actuation systems for fully wearable assistive devices: Requirements, selection, and optimization for out-of-the-lab application of a hand exoskeleton," *Front. Robot. AI*, vol. 7, 2021, Art. no. 596185.
[39] V. Agrawal, W. J. Peine, and B. Yao, "Modeling of transmission characteristics across a cable-conduit system," *IEEE Trans. Robot.*, vol. 26, no. 5, pp. 914–924, Oct. 2010.
[40] S. Buchanan and F. Sergi, "Dynamic modeling and state estimation of cable-conduit actuation during interaction with nonpassive environments," *IEEE/ASME Trans. Mechatron.*, vol. 26, no. 5, pp. 2462–2471, Oct. 2021.
[41] X. Li, J. Liu, W. Li, Y. Huang, and G. Zhan, "Force transmission analysis and optimization of Bowden cable on body in a flexible exoskeleton," *Appl. Bionics Biomech.*, vol. 2022, 2022.
[42] Q. Wang, K. Yuan, J. Zhu, and L. Wang, "Walk the walk: A lightweight active transtibial prosthesis," *IEEE Robot. Automat. Mag.*, vol. 22, no. 4, pp. 80–89, Dec. 2015.
[43] Y. Feng, J. Mai, S. K. Agrawal, and Q. Wang, "Energy regeneration from electromagnetic induction by human dynamics for lower extremity robotic prostheses," *IEEE Trans. Robot.*, vol. 36, no. 5, pp. 1442–1451, Oct. 2020.
[44] J. Zhang et al., "Human-in-the-loop optimization of exoskeleton assistance during walking," *Science*, vol. 356, no. 6344, pp. 1280–1284, 2017.
[45] J. Camargo, A. Ramanathan, W. Flanagan, and A. Young, "A comprehensive, open-source dataset of lower limb biomechanics in multiple conditions of stairs, ramps, and level-ground ambulation and transitions," *J. Biomech.*, vol. 119, 2021, Art. no. 110320.
[46] A. N. Lay, C. J. Hass, T. R. Nichols, and R. J. Gregor, "The effects of sloped surfaces on locomotion: An electromyographic analysis," *J. Biomech.*, vol. 40, no. 6, pp. 1276–1285, 2007.
[47] Z.-Y. Cai et al., "Comparison of lower limb muscle activation during downhill, level and uphill running," *Isokinetics Exercise Sci.*, vol. 18, no. 3, pp. 163–168, 2010.
[48] L. Hunter, E. Hendrix, and J. Dean, "The cost of walking downhill: Is the preferred gait energetically optimal?," *J. Biomech.*, vol. 43, no. 10, pp. 1910–1915, 2010.
[49] J. R. Franz and R. Kram, "The effects of grade and speed on leg muscle activations during walking," *Gait Posture*, vol. 35, no. 1, pp. 143–147, 2012.
[50] C. Wang et al., "Design of an ankle exoskeleton that recycles energy to assist propulsion during human walking," *IEEE Trans. Biomed. Eng.*, vol. 69, no. 3, pp. 1212–1224, Mar. 2022.
[51] F. A. Panizzolo et al., "A biologically-inspired multi-joint soft exosuit that can reduce the energy cost of loaded walking," *J. Neuroengineering Rehabil.*, vol. 13, no. 1, pp. 1–14, 2016.
[52] Y. Ding et al., "Biomechanical and physiological evaluation of multi-joint assistance with soft exosuits," *IEEE Trans. Neural Syst. Rehabil. Eng.*, vol. 25, no. 2, pp. 119–130, Feb. 2017.
[53] Z. Wang, C. Chen, F. Yang, Y. Liu, G. Li, and X. Wu, "Real-time gait phase estimation based on neural network and assistance strategy based on simulated muscle dynamics for an ankle exosuit," *IEEE Trans. Med. Robot. Bionics*, vol. 5, no. 1, pp. 100–109, Feb. 2023.
[54] G. Durandau, W. F. Rampeltshammer, H. van der Kooij, and M. Sartori, "Neuromechanical model-based adaptive control of bilateral ankle exoskeletons: Biological joint torque and electromyogram reduction across walking conditions," *IEEE Trans. Robot.*, vol. 38, no. 3, pp. 1380–1394, Jun. 2022.
[55] X. Tan, B. Zhang, G. Liu, X. Zhao, and Y. Zhao, "A time-independent control system for natural human gait assistance with a soft exoskeleton," *IEEE Trans. Robot.*, vol. 39, no. 2, pp. 1653–1667, Apr. 2023.

Ming Xu (Graduate Student Member, IEEE) received the B.E. degree in mechanical design, manufacturing, and automation from the China University of Petroleum, Qingdao, China, in 2020, and the M.E. degree in mechanical engineering in 2023 from Peking University, Beijing, China, where he is currently working toward the Ph.D. degree in dynamics and control with the College of Engineering.

His research interests include wearable robots and human–robot interaction.

Zhihao Zhou (Member, IEEE) received the B.E. degree in mechanical design, manufacturing, and automation from the China University of Geosciences, Beijing, China, in 2012, and the Ph.D. degree in dynamics and control from Peking University, Beijing, China, in 2017.

He was a Postdoctoral Researcher with the Beijing Innovation Center for Engineering Science and Advanced Technology. He is currently an Assistant Professor with the Institute for Artificial Intelligence, Peking University. His research interests include wearable systems and rehabilitation robots.

Zezheng Wang received the B.E. degree in automation from Beihang University, Beijing, China, in 2022. He is currently working toward the Ph.D. degree in dynamics and control with the College of Engineering, Peking University, Beijing.

His research interests include bionic robots, prescribed performance control, and fuzzy control.

Lecheng Ruan received the B.S. (Hons.) degree in robotics from the School of Mechatronic Engineering, Harbin Institute of Technology, Harbin, China, in 2015, and the Ph.D. degree in robotics from the Department of Mechanical and Aerospace Engineering, University of California, Los Angeles, CA, USA, in 2020.

He is currently with the National Key Laboratory of General Artificial Intelligence, Beijing, China, and Peking University, Beijing. His research interests include control and optimization, mechatronics, robotics, perception, and signal processing.

Jingeng Mai received the B.E. degree in electrical engineering and automation from the China University of Geosciences, Beijing, China, in 2005, and the M.Sc. degree in control theory and control engineering from Peking University, Beijing, in 2008.

He joined Peking University as a Postdoctoral Researcher in 2016. He is currently an Associate Professor with the College of Engineering, Peking University. His research interests include intelligent manufacturing and robotics.

Qining Wang (Senior Member, IEEE) received the Ph.D. degree in dynamics and control from Peking University, Beijing, China, in 2009.

He is currently a Full Professor with the College of Engineering, Peking University. He is also the Vice-Dean with the College of Engineering, Peking University. He has authored/coauthored more than 200 scientific papers in international journals and refereed conference proceedings. His research interests include wearable robotics and human–machine interfaces.

Prof. Wang was an Associate Editor for IEEE ROBOTICS AND AUTOMATION MAGAZINE from 2016 to 2018, and a Technical Editor for IEEE/ASME TRANSACTIONS ON MECHATRONICS from 2017 to 2020. He has been an Associate Editor for *Robotica* since 2018 and IEEE TRANSACTIONS ON MEDICAL ROBOTICS AND BIONICS since 2018.